# Thermal insulation and flammability of composite waste polyurethane foam encapsulated in geopolymer for sustainable building envelope

Barbara Horvat [a,*], Nataša Knez [a], Uroš Hribar [b], Jakob König [b], Branka Mušič [a]

[a] *Slovenian National Building and Civil Engineering Institute, Ljubljana, Slovenia*
[b] *Jožef Stefan Institute, Ljubljana, Slovenia*

## ARTICLE INFO

## ABSTRACT

Polyurethane foam (PUR) is a lightweight, thermally insulating, widely used, and highly flammable material that has after its use an adverse effect on the environment, i.e., PUR disposal is considered hazardous. Its flammability can be mitigated using various fire retardants, but they do not change the hazardous nature of waste PUR. Therefore, in the current study, waste PUR with and without flame retardants based on N and P was incorporated into a geopolymer, the alkali-activated material (AAM) based solely on metakaolin, to evaluate the potential recycling route of waste PUR while taking into account its flammability, so it can enter safely into the circular economy through the building industry. To enhance the mechanical properties of the composite, a fresh mixture was irradiated with microwaves. However, the irradiation of geopolymer containing PUR negatively influenced mechanical performance, which led to the evaluation of the behaviour of the complex dielectric constant of PUR and fire retardants. Materials and composites were evaluated regarding their chemistry, mineralogy, micro-structure, and porosity to connect the structure with extrinsic properties like geometrical density, thermal conductivity, and fire properties. Nonetheless, positive influences of PUR being encapsulated in the geopolymer were lowered density (from 1.8 to 1.6 kg/l) and improved thermal insulation ability (from 940 to 860 mW/(m·K)) of the composites: with the inclusion of <5 % of PUR, thermal insulation improved by nearly 10 %. However, the contribution of PUR to the composite originated from its skeleton, which has more than 15 times bigger geometrical density (0.81 kg/l) compared to the density of the skeleton (0.047 kg/l). This offers an open field for further advancements of thermal properties, but would also lead to a decrease of the compressive strength, which was already lowered from 90 MPa for 30 % with <5 % of added grated PUR. Furthermore, the flammable nature of PUR and its other drawbacks can be controlled by permanent embedding in the noncombustible structure of geopolymer, making the envelope of sustainable buildings green and safer. Overall, including grated waste PUR in geopolymer represents a promising, easy, cost-effective recycling path with low energy consumption, where the composite cannot develop fire on a scale of pure PUR, even in the worst-case scenario, but only if the composite is designed in a way, that flammable materials cannot join flames during their combustion. This paper gives prospects to other flammable waste materials to be safely used in the circular economy, and to porous materials to shape properties of the composite by their intrinsic and/or extrinsic properties.

## 1. Introduction

Polyurethane foam (PUR) is a lightweight organic polymer made from polyols and isocyanates. This organic foam accounts for nearly 70 % of global polyurethane consumption and 50 % of the polymer foam market (Szycher, 2013) owing to its several advantages: It bonds easily with various materials, is dimensionally stable, can be easily cut into any shape, has low density, is resistant to water and several other chemicals, is chemically and biologically inert, withstands heat and cold, and cures at ambient conditions. Furthermore, it is a widely used material in the building and civil engineering sector as a thermal, sound, and electrical insulator. In addition, it is employed as an adhesive and for soil reinforcement. It is also extensively used for transportation and in furniture products (Grolms, 2019; Mušič et al., 2022). However, it has a few disadvantages, such as sensitivity to light, susceptibility to biodegradation by certain microbes and fungi, and combustibility. Its high flammability is particularly concerning and represents a significant

challenge (Günther et al., 2018).

Therefore, to decrease the flammability, different flame retardants are added to PUR (Mušič et al., 2022) to prevent, suppress, and delay the development of flames and prevent, or at least restrain and limit the spread of fire. Flame retardants can be inorganic or organic compounds containing at least one of the following chemical elements: halogens Cl, Br, F, and I, and non-halogens P and N. The use of halogen-based flame retardants is increasingly restricted owing to growing concerns and evidence of their harmful effects on the environment and human health. Nonetheless, despite the replacement of flame retardants based on halogens with environmentally friendly materials like ammonium polyphosphates (APP) and 2,4,6-triamino-1,3,5-triazine (TATA) (Mušič et al., 2022), PUR is still considered environmentally critical, and classified as hazardous waste (Grolms, 2019). Thus, PUR as waste is either incinerated or landfilled, as recycling is still more of a subject of ongoing research than a widely implemented practice (chemical solutions are expensive and use a lot of energy and toxic chemicals (Grolms, 2019)). However, incineration of PUR releases different hazardous chemicals (isocyanates, hydrocyanic acid, and dioxins), and when landfilled, PUR decomposes into substances that harm the environment (Grolms, 2019).

Although PUR and organic flame retardants may not be ideal precursors (reagents) for alkali-activated reactions, they might be at least safely stored in alkali-activated materials (AAMs) as fillers. AAMs are produced from any material (whether natural resources or secondary materials) that contains sufficient Si and Al in amorphous content, which dissolve in strong alkali solutions (usually hydroxides and alkali silicate solutions) and chemically bind into an aluminosilicate network (ASN) (Škvára, 2007). If AAM is prepared so that the molar ratio of the amorphous *(1st group of the periodic system):Al* does not exceed 1, efflorescence can be avoided (Longhi et al., 2020) and chemical reactions in AAM can settle sooner (Horvat and Ducman, 2019). In chemically stable AAM, the ASN can store nearly any type of filler. This ranges from sand, which can reduce the amount of binder (a commonly used alternative term for the ASN) in the AAM without loss of mechanical strengths (sand represents hard material) (Pavlin et al., 2022), to any type of lightweight filler (Traven et al., 2022). Even pores can be considered as lightweight filler, i.e., they are filled with gas (Ducman and Korat, 2016; Horvat and Ducman, 2019), which enhance the thermal insulation performance of AAM while losing the high(er) mechanical strength. It can safely immobilise hazardous waste (hazardous elements in slags (Deja, 2002; Yunsheng et al., 2007), intermediate-level wastes (Khalil and Merz, 1994), fly ash (Nikolić et al., 2014, 2017 etc.) and radioactive waste (Fernandez-Jimenez et al., 2005; Guangren, 2002).

Also geopolymer (AAM where precursor contains Al, Si and hardly any Ca (Marvila et al., 2021)) offers a potential "black hole" for the "consumption" of waste materials (Mohajerani et al., 2019; Podolsky et al., 2021). No matter the technique used: moulding or 3D-printing (Qaidi et al., 2022). However, as reported (Podolsky et al., 2021), many studies are not focusing on the optimal Si:Al:Na (Duxson et al., 2005) ratio which influences geopolymer properties and affects the potential of the addition of waste materials, nor their final compressive strength is not modelled (Ahmed et al., 2023). However, the algorithm that focuses on the design of the mixture (precursor and alkali) with the optimal Si:Al:Na ratio, for any material, not just metakaolin, and for any alkali was reported (Horvat and Ducman, 2019). In the literature, the terminology "geopolymer" is still misused: many studies reporting consumption of waste by "geopolymer" are about AAM (precursor has more Ca than Si and Al together (Marvila et al., 2021)) made from waste materials that react with alkali (but chemically form different ASN compared to the geopolymer (Davidovits, 1989)). The number of studies reporting "geopolymer" consumption of in-alkali-reactive waste (Kheimi et al., 2022) is far superior compared to the geopolymer consumption of in-alkali-inert waste (Skariah Thomas et al., 2022). However, among weakly or non-reactive additives in geopolymer are different fibres (non-metallic (Moradikhou et al., 2020) and metallic (R. A. Sá Ribeiro, 2017)), aggregates (also recycled (Zaid et al., 2022)), vehicle tires (rubber) (Albidah et al., 2022; Dos Reis Ferreira et al., 2024), waste rubber from electrical cables (Horvat and Mušič, 2023), natural graphite (Nadi et al., 2023), single minerals (Kohout and Koutník, 2020) etc. Indeed, AAM (geopolymer included) not only can store versatile solid materials (and gasses) in its structure, but it also exhibits the potential to be used as a thermal (Łach et al., 2016; Prud'homme et al., 2015) and an acoustic insulator (Chen et al., 2022; Zhang et al., 2015) when containing lower-density inclusions (Le Roy et al., 2005). In addition, AAM is noncombustible, making it a fire-resistant material (Jow et al., 2015; Yang et al., 2012). Moreover, it can be used as a flame-resistant coating to protect steel (Sarazin et al., 2021). Therefore, embedding PUR in AAM may suppress the fire behaviour of PUR.

However, there are limited studies involving AAMs and "building and civil engineering" PURs reported to date. Chen et al. has focused on a composite of geopolymer (AAM based only on metakaolin, MK) and polyurethane sponge (Chen and Lee, 2018). This composite showed distinct crack propagation and destruction behaviour after exposure to compressive loads. Notably, polyurethane sponge is flexible and finds application in bedding, furniture, and packaging, thus providing comfort to users. Conversely, "building and civil engineering" PURs serve entirely different purposes, like for sound and thermal insulation, as air barrier sealants around windows and doors, but can be found also in sports equipment (surfboard blanks) (Grünbauer et al., 2004). The difference in properties between rigid and flexible foam come from different molar ratios between isocyanates and polyols (Gogoi et al., 2014), but a comparable study between both embedded in geopolymer was not reported yet.

Flexible polyurethane sponge, cut into small pieces (size not reported, from photography it seems bulk), was added into "geopolymer" (alkali-activated material from fly-ash and ground granulated blast furnace slag): (i) only cut, (ii) cut, dipped in phase change material (labelled in the paper as RT-31) and coated with "geopolymer" paste. It was reported that (ii) exhibited lower compressive strength than the reference sample without any foam, but (i) the sample with not-coated foam showed higher or similar compressive strength to the sample without any foam, even when the volumetric addition of foam was 75 %, which would need to be repeated by another laboratory for confirmation (Hassan et al., 2019).

Polyurethane rubber, cut on bulk pieces (triangular shape, around 2 cm according to the photograph), replaced coarse aggregate (measuring 2 cm; replacement is reported to be up to 20 %, while in the conclusion to be up to 50 %) in "geopolymer" concrete from fly ash, fine and coarse aggregate. While fresh compressive strengths are smaller for "geopolymer" concrete with polyurethane rubber, their 28-day-old are comparable to samples with coarse aggregate only. However, the conclusion is not backed up by the results, although logical, that rubber cannot be used to increase the strength of the concrete (Pandya et al., 2017).

In addition to using polyurethane sponge, rubber polyurethane and pulverised rigid PUR in the geopolymer, Garces et al. calculated life cycle assessment (LCA) for the AAMs from coal fly ash, ground granulated blast furnace slag, and their combination. With the addition of self-healing agents in microcapsules (Garces et al., 2021), including poly (urea-urethane), synthesized through interfacial polymerisation (Beglarigale et al., 2018). However, self-healing is only predicted to happen through the reaction between unreacted precursors and alkali activators. But in general, the amount of alkali should be kept lower than needed to avoid efflorescence (Horvat and Ducman, 2019).

The most similar study to ours was mixing geopolymer slurry with polyurethane foam and polyisocyanurate foam in powder form (the procedure of pulverization and fines of organic material is not mentioned; according to the photograph, the polyurethane powder material is not bulk). However, the geopolymer mixture was not determined by the chemistry and mineralogy of the metakaolin and used alkalis. Polyurethane was added to the mixture to 20 % calculated on the mass of metakaolin, the mixture was cured at 40 °C for 24 h. The study reported improvement in thermal conductivity with the highest addition of polyurethane. Regarding compressive strength mentioned in the abstract, introduction and conclusions, there are no reported results in the paper, just the punching strength for thin layers (Bergamonti et al., 2018).

Nonetheless, from published studies on geopolymer (or AAM) with the addition of PUR, no conclusion on the design of composites to gain prechosen properties is reported: not even the span of the geometrical density of the composite, which influences thermal and mechanical properties. As well as there is no information about containing the flammability under control with embedment in the ASN. Therefore, to dive into the challenge(s), PUR without flame retardant (PUR-0), PUR with APP (PUR-1) and PUR with TATA (PUR-2) (Mušič et al., 2022), gently grated below 1 mm, were incorporated into geopolymer and Na-silicate solution (Horvat et al., 2022a, 2023) to lower its density and improve thermal performance. With such processing, the need to foam with expensive, pure, and health-hazardous chemicals (Horvat and Ducman, 2019) that substantially increase LCA (Atienza and Ongpeng, 2022) is avoided, and at the same time waste PURs get safely incorporated in geopolymer. When trying to avoid the loss in mechanical performance due to PUR incorporation in the geopolymer, a fresh mixture was irradiated with microwaves at low power (Horvat et al., 2023), which led to the conclusion that the influence of the microwaves on composites can be positively or negatively enhanced just by exclusion or inclusion of smaller amounts of additives. However, this study shows that by cost-effective and straightforward recycling of PURs in the geopolymer, it is possible to mitigate the major drawbacks of the PUR

and extend its use in the building industry products like façade elements for the sustainable building envelope.

## 2. Materials and methods

For the development of the composite, geopolymer (Horvat et al., 2022b) and PUR (Mušič et al., 2022) used were developed in our previous studies. The mixture used for geopolymer did not show any efflorescence over 3 years and had the highest compressive strength among tested mixtures. On the other hand, PUR was used as waste material. Preparation of materials and experimental timeline is presented in Supplement 2 in Fig. S0.

### 2.1. Ingredients, PUR and geopolymer

All solid ingredients used in the composite preparation are shown in Fig. 1, including their photographs and scanning electron microscopy (SEM) micrographs. As metakaolin (MK) was used in its as-received state (powder of random rocky-like shapes with an average diameter 12.4 μm evaluated using SEM; distribution and statistics are in Supplement 3), porous waste PUR-0 (PUR without any addition of flame retardant), PUR-1 (PUR with flame retardant ammonium polyphosphates, APP, which is blocky-shaped powder with smooth edges and average diameter 13.6 μm evaluated using SEM; distribution and statistics are in Supplement 3), and PUR-2 (PUR with flame retardant 2,4,6-triamino-1,3,5-triazine, TATA, which is random rocky-like shaped with sharp edges and average diameter 14.8 μm evaluated using SEM; distribution and statistics are in Supplement 3) were gently grated (to avoid any increase in the temperature to avoid degradation of chemical bonds) and sieved below 1 mm. These PUR wastes (shown in more detail in Supplement 2 in Fig. S3 as SEM micrographs, and in Table S2 with energy-dispersive X-ray spectroscopy (EDXS) performed on inorganic impurities and organic PURs) were remnants particularly prepared for a previous study investigating the impact of flame retardants on the flammability of PUR (short description of the procedure is in the Supplement 2) (Mušič et al., 2022), and had been stored in the dark at room conditions for over a year. Their grated mixture, PUR$_{mix}$, was used for preliminary experiments. However, all the porous structure of grated PURs was completely destroyed, as is shown in Figs. 1 c-2) to c-4). Their surface is shown in Supplement 2 in Fig. S3, as well as the inclusion of APP and TATA in the structure of PUR. Their bulk properties, published in our previous study (Mušič et al., 2022), used for comparison with synthesized composites in this study and calculations of densities of composites, are.

- PUR-0: geometrical density 0.047 kg/l, bulk density 0.095 kg/l, skeletal density 0.81 kg/l, thermal conductivity 365 mW/(m·K), total porosity 88.3 %;
- PUR-1: geometrical density 0.063 kg/l, bulk density 0.085 kg/l, skeletal density 0.32 kg/l, thermal conductivity 364 mW/(m·K), total porosity 73.5 %;
- PUR-2: geometrical density 0.063 kg/l, bulk density 0.080 kg/l, skeletal density 0.27 kg/l, thermal conductivity 356 mW/(m·K), total porosity 70.9 %.

In our previous study, a detailed procedure was presented for the determination of the ideal mixture for geopolymer with no efflorescence, the highest possible compressive strength, and the lowest possible amount of alkali used (Horvat and Ducman, 2019), which was used also on MK from this study. Two potential mixtures were presented in the scope of the project of microwave irradiation of alkali-activated materials (Horvat et al., 2022b), a mixture that gave the highest compressive strength, labelled MK$_b$, is used also in the following study with the same abbreviation.

For determining the optimal mixture for geopolymer using the chosen precursor (MK) and alkali (Na-silicate solution, Geosil, 344/7,
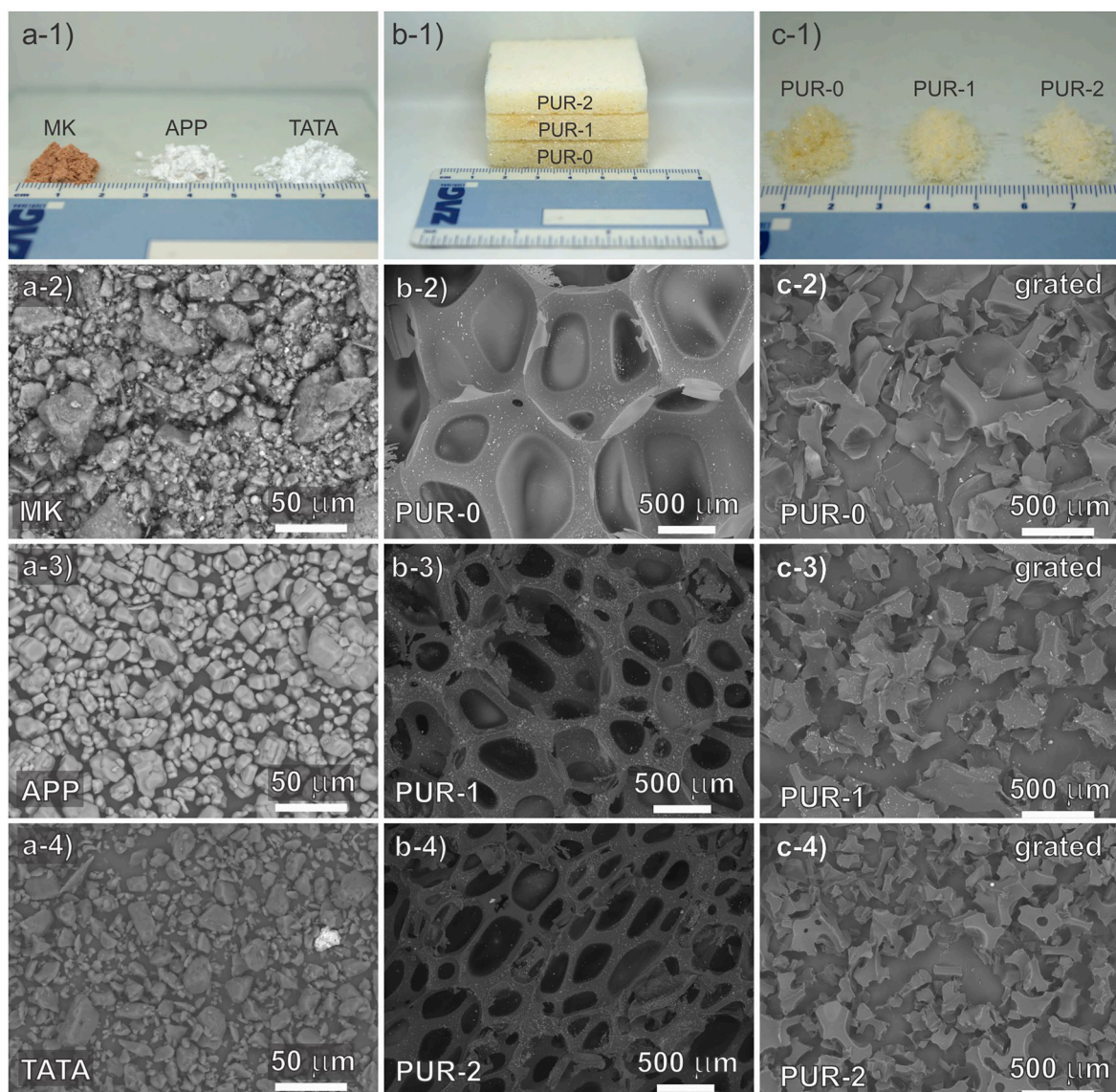
**Fig. 1.** Photographs and micrographs of a) solid ingredients used for composite material synthesis, i.e., precursor MK, fire retardants present in PUR-1 and PUR-2, APP and TATA, respectively. b) Solid PUR-0, PUR-1, and PUR-2 (for SEM gently polished up to the 4000-grit sandpaper) and c) their grated counterparts. SEM magnification in a) is 500, in b) and c) is 40.

Woelner, Ludwigshafen, Germany, 16.9 % $Na_2O$, 27.5 % $SiO_2$, the rest is $H_2O$; the alkali was used as received and as only alkali), MK underwent the following analyses.

- Gravimetric analysis was performed on MK to determine the amounts of organic and carbonate materials: MK was dried (at 105 °C for 24 h in a heating chamber WTB Binder; to remove water), then ignited at 550 °C for 2 h (to evaluate the organic compound), and then at 950 °C for additional 2 h (to evaluate the amount of carbonates). After every step samples were weighted and loss on ignition (LOI) was calculated as the loss of mass. Results were used for calculation of the optimal mixture with chosen alkali and are presented in the Supplement 2.
- X-ray fluorescence (XRF; Thermo Scientific ARL Perform'X Sequential XRF; measures from chemical element F to Am) was performed on material ignited at 950 °C and melted into a disc to determine all elements present in MK. For melting of MK into discs after ignition at 950 °C, MK was mixed with Fluxana (Fluxana(s) FX-X50-2, a mixture of lithium tetraborate and lithium metaborate in mass ratio 1 to 1) to lower the melting point, and with $LiBr_{(l)}$ (50 ml $H_2O$ and 7.5 g of LiBr

(s) from Acros Organics) to prevent glueing of the melt onto the Pt crucible. Measured XRF data were analysed using UniQuant 5 and are presented in the Supplement 2.

- X-ray powder diffraction (XRD; Empyrean PANalytical X-ray Diffractometer, Cu X-Ray source) along with Rietveld refinement using external standard (corundum, $Al_2O_3$) and software X'Pert Highscore plus 4.1 was performed in $2\theta$ range from 4 to 70°, and in step 0.0263°, to determine which minerals are present in MK, their amounts, and the amorphous content. Results for MK are shown in the Supplement 2 and were used for the calculation of the optimal mixture to avoid efflorescence.

Results of LOI, XRF and XRD for MK were reported in our previous study (Horvat et al., 2022b, 2023) and can be found also in Supplement 2 Fig. S1 (XRD pattern of MK) and Table S1 (XRF and Rietveld refinement results are shown per present chemical elements without O), as well as the optimal mixture of ingredients for alkali activation, which was set to fulfill the condition of the final molar ratio of amorphous content in the alkali-activated material *Si:Al = 1.9:1* and *(sum of elements in the 1st group of the periodic system):Al < 1*. The mixture in mass ratios, $MK_b$,

shown in Table 1, was calculated using software developed in project No. C3330-17-529032 "Raziskovalci-2.0-ZAG-529032" and upgraded in the ARIS project under Grant No. J2-3035.

Besides the theoretical calculation of the mixture that would be chemically optimal, the viscosity of the fresh slurry was monitored using a viscometer (Haake PK 100, VT 500 with detector PK2 1.0° at 25 °C; plate-plate geometry, with diameter 2 cm, and distance between plates 0.3 mm; with measurement protocol: 60 s upwards ramp (shear rate from 0.13 to 400 s$^{-1}$), 30 s hold time (shear rate 400 s$^{-1}$), and 60 s downwards ramp (shear rate from 400 to 0.13 s$^{-1}$)) to test if additional liquid should be introduced into the system or if it the liquid can be further decreased, i.e. too much liquid leads to lower mechanical strengths (Horvat et al., 2022b; Horvat and Ducman, 2019). The goal was to keep the viscosity of the still workable slurry (it can still be mixed into a compact slurry, and not into wetted aggregates) in the "torque overload" region, i.e., when torque value exceeds 115 % of the maximum torque, which is when the motor blocks due to overload protection.

### 2.2. Composite

A grated mixture of PUR-0, PUR-1, and PUR-2, mixed in mass percentage 1:1:1, PUR$_{mix}$, was first mixed with powder MK, and then used to experimentally determine the amount of optimal addition of PUR in the geopolymer, mixtures MK$_b$ PUR$_{mix}$, by considering the workability of the slurry during mixing and moulding, and geometrical density ($\rho_G$) and mechanical properties of composites. The chosen grated amount was mixed with MK as pure systems, i.e., as MK and PUR-0 (geopolymer mixture MK$_b$ PUR-0), as MK and PUR-1 (geopolymer mixture MK$_b$ PUR-1), and as MK and PUR-2 (geopolymer mixture MK$_b$ PUR-2), as shown in Table 1. The final selection of using 3 g of pure PURs (as much as possible) is better described in the results section, however, mixing into a standard slurry-like mixture was already challenging with the addition of 4 g of PUR (it ended in a big wet "aggregate"), but the addition of 5 g ended in lots of smaller wet "aggregates" that could not bind together into a whole just with mixing (too much solid for the amount of used liquid). This changes the type of moulding (additional force) and represents a potential new parameter. However, all samples were "shaped" into the same-looking product without using excessive force. The amount of added PURs, presented in Tables 1 and is shown in mass percentages (m%) calculated on slurry (solid MK and alkali) and on geopolymer (solid MK, alkali without H$_2$O) after complete dehydration. The first ratio of organic to inorganic material represents the m% of PUR at the beginning of synthesis, and the last one at the end of reactions, which is a theoretical limit. The chosen ratio of added pure PURs was below 5 m%.

The solid materials were mixed separately while aiming for a homogenous mixture, then the solid mixture was added to a liquid alkali and mixed with an overhead stirrer at up to 1000 rpm (Witeg Laboratory Agitator HT-50AX). Every batch (50 g MK, 33 g alkali, and PUR) was prepared separately so that slurries went through the same procedure at

**Table 1**
Masses of the used ingredients with mass percentage (m%) of PUR normalised on alkali-activated slurry with and without water. Mixture MK$_b$ was evaluated in a previous study (Horvat et al., 2022b). Alkali is a commercial Na-water glass.

| Mixture | MK [g] | Alkali [g] | Grated PUR [g] | Grated PUR in slurry in m% [%] | Grated PUR in geopolymer (slurry without H$_2$O) in m% [%] |
|---|---|---|---|---|---|
| MK$_b$ | 50 | 33 | / | 0 | 0 |
| MK$_b$ PUR$_{mix}$ | 50 | 33 | 1/2/3/4/5 | 1.2/2.4/3.5/4.6/5.7 | 1.5/3.0/4.4/5.8/7.2 |
| MK$_b$ PUR-0/1/2 | 50 | 33 | 3 | 3.5 | 4.4 |

approximately the same age. From every batch half of the slurry was irradiated and half was cured at room conditions only, to minimize other parameters on the mechanical strength except for the type of curing (this procedure was repeated 3 times for every batch). Because the amounts were small, mixing was finished in 1.5 min. For upscaled samples, mixing had to be prolonged to ~3 min.

Mixed solid and liquid ingredients were immediately cast into silicone moulds of size (2 × 2 × 8) cm$^3$ (for mechanical tests) and (10 × 10 × 4) cm$^3$ (for thermal and fire characteristics evaluation). Half of the samples used for mechanical tests and all samples prepared for thermal and fire behaviour tests were irradiated with microwaves at 100 W for 1 min (μ - abbreviation is denoting curing with microwave irradiation; frequency 2.45 GHz, inverter microwave, Panasonic, NN-CD575M), smaller samples 3 min after start of the mixing, bigger ~5 min after start of the mixing (mixing and moulding of bigger amount took more time). Smaller samples were put individually into the 1st observed dosimetry maxima position (~6 cm from the centre of the turntable (Horvat et al., 2022a), where the material can be heated by exposure to microwaves, which was evaluated on the cheese placed evenly on rotating and still turntable), while larger samples were put into the centre of the turntable, all in the open moulds (Horvat et al., 2023). All samples were further cured at room conditions (T$_0$ - abbreviation is denoting curing at room conditions; 55 % moisture, 22 °C) for 14 d before mechanical, chemical, and mineralogical evaluation, thermal conductivity ($\lambda$) measurement, and additional treatment at elevated temperatures (last was performed to be able to connect the fire behaviour results with changes in the material; 250 °C for 2 h in the heating chamber Memmert, and 500, 750, and 1000 °C for 2 h, with the increase rate 10 °C/min to the selected temperature in the furnace Protherm, but only samples that were irradiated with microwaves). However, reaction to fire was tested on 2-month-old samples to allow the material to completely settle regarding its moisture content (not allowing un-evaporated water to influence the results).

### 2.3. Methods for analysis of ingredients and composite

On all ingredients as well as on composites, the following tests were performed.

- Fourier-transform infrared (FTIR) spectroscopy (PerkinElmer Spectrum Two, ATR mode), from 380 to 4000 cm$^{-1}$, in steps 4 cm$^{-1}$, using software PerkinElmer Spectrum (Version 10.03.07). Analysis was performed on pulverised dry materials and on liquids, to follow the presence of the organic material in the composite;
- XRD, where 2θ ranged from 4° to 70°, in step 0.0263°, was performed on pulverised materials in the same manner as for MK, to determine mineralogical stability and changes upon heat treatment;
- Scanning electron microscopy (SEM; Jeol JSM-IT500; 20 kV, low vacuum conditions, 60 Pa) with backscattered electron detector in shadow (BED-S) mode on uncoated powder ingredients, gently polished PUR-0, PUR-1, and PUR-2 up to sandpaper-grit 4000 (Fig. 1), and cross-section of composites after mechanical tests, to visualise the changes in the composite upon heat treatment and the encapsulation quality of the PUR in the aluminosilicate network of the geopolymer.

In addition to the aforementioned tests, solely on composites, additional analyses were performed that are crucial for the safety of the building industry products when used in real-life settings and for understanding the influence of PUR inclusion in the composite.

- $\rho_G$ was calculated as a ratio between mass and volume of each sample by using 2 decimal scale and electronic callipers (Mitutoyo, Digimatic calliper) just before mechanical test evaluation;
- The mechanical performance of 14-day-old composites was measured with compressive and bending strength testing machine

(ToniTechnik, ToniNORM; force detection limit 10 kN and 300 kN for bending and compressive strength measurement, respectively); with a force application rate of 0.10 kN/s and 1.20 kN/s for bending and compressive strength measurement, respectively;

- Distribution of pores, as well as bulk ($\rho_B$) and skeletal ($\rho_S$) densities, were evaluated using mercury intrusion porosimetry (MIP; Micromeritics autopore IV, mercury porosimeter, Series 9500) on non-destroyed samples kept at 70 °C from after mechanical tests measurement till the MIP measurement (small pieces of samples tested did cool down to the room temperature before the measurement) – all samples were older than 1 month;

- Effective $\lambda$ was determined using the hot-disk method (HotDisk TPS 2500 S Thermal Constants Analyser) on samples cut in half. In those halves, a Kapton-insulated sensor with a 9.9 mm radius was placed (the largest sensor available was used to obtain an average $\lambda$ to avoid any potential effect of heterogeneities in the samples (pores)). Measurements were performed with a specific heating power of 175 mW for a duration of 160 s, to obtain probing depths within the sample's dimension (the method assumes that the samples are isotropic and infinitely large);

- Reaction to fire was analysed using a cone calorimeter (Fire testing technology) according to the standard ISO 5660–1:2015. Samples of size $(10 \times 10 \times 4)$ cm$^3$ (as also powders evenly spread in the metallic mould of size $(10 \times 10 \times 4)$ cm$^3$) were exposed to the heat flux of 50 kW/m$^2$, where the closest part of the heat source was 2.5 cm away from the sample. The sample is heated with irradiation and starts to emit pyrolysis gases (unless it is incombustible), which ignite by a spark igniter positioned above the sample. The standard is used to evaluate the heat release rate and dynamic smoke production;

- Released gasses during fire tests in the cone calorimeter were measured using an FTIR spectroscopy analyser (atmosFTIR; Protea) according to the standard ISO 19702:2015, which is used as guidance for sampling and analysis of released gases in small and large-scale fire tests.

Bulk samples on which fire tests were performed exhibited different $\rho_G$, heights, and masses, i.e., only the surfaces exposed to the heat source and distances between the heat source and sample were equal among the tested samples. To compare the release of gasses and smoke production from the composite materials more realistically, results obtained using atmosFTIR and cone calorimeter were factorised to the biggest mass among all tested geopolymer samples (multiplication by biggest mass, MK$_b$, and division by sample's own mass), i.e., sample masses were set to be the same. In addition to multiplying results, their negative values were filtered, i.e., set to 0. By contrast, the positive part of the white noise (along with the signal) was left unfiltered, i.e., it was just multiplied by the mass factor. For comparison of the severity of the fire results and estimation, if the results were most likely just white noise, our already published results for PUR-0, PUR-1 and PUR-2 (Mušič et al., 2022) (heat flux was just 40 kW/m$^2$, while samples tested for this study were exposed to stronger heat flux, i.e., 50 kW/m$^2$) were factorised and filtered in the same way as were the fire measurements of geopolymer composites. The formula used on the data set is provided in the Appendix, Eq. (A.1).

The amount and "quality" of the fire fuel (PUR in this study) define the time behaviour of the measured fire curves, but the curve integral for the same sample of another mass is calculable just by mass factorisation (multiplying by chosen mass and dividing by its own) regardless of how the time curve behaved. Therefore, to compare the influence of geopolymer on the flammability of PUR and suppressing the fire by insulating PUR in its own structure, masses of PUR in the bulk materials (geopolymer composites in this study and PURs from our previous study (Mušič et al., 2022)) were set to be equal (10 g). Results from the cone calorimeter and atmosFTIR for PUR were factorised by dividing the chosen mass of PUR (10 g) by its real mass, while for the mass factor for geopolymer composites the mass of PUR in the sample was calculated as

no water would evaporate from the mixture (which is the lowest amount possible in the composite). Notably, more PUR in geopolymer implies a smaller multiplication factor and a decrease in fire curve values after factorisation. This would be a desirable result, but it is an artificial decrease in fire results and not the worst-case scenario. The formula used on the data set is provided in the Appendix, Eq. (A.2) and Eq. (A.3).

On samples subjected to elevated temperatures for 2 h, in addition to mechanical performance evaluation along with $\rho_G$, FTIR, XRD, SEM, and MIP analyses were performed to gain insights into the behaviour of the composite material at the chosen temperatures.

Because geometrical densities of the composites did not obey the classical formula of taking into account geometrical densities of the ingredients and their masses, MIP data for PUR-0, PUR-1 and PUR-2 were used, besides their geometrical densities, to calculate their densities and create a model on how to experimentally make a composite with desired density when using porous material like PUR.

Because of the unique and non-expected behaviour of the mechanical performance of composites with PURs irradiated with microwaves, the complex dielectric constants (permittivity) of all additives were measured in relation to frequency. This was accomplished using the vector network analyser (VNA; PNA Network Analyser E8361C, Agilent Technologies, 10 MHz–67 GHz), operating in the range of 10 MHz to 8 GHz coupled with an open-ended coaxial probe. The probe was dipped into powders APP, TATA, and into grated PURs. PURs were also evaluated as a cube of approximate size $(5 \times 5 \times 5)$ cm$^3$, where the probe was once gently positioned and once firmly pressed onto the sample surface. The probe was also pressed onto the thin PUR envelope that forms as an outer layer between the PUR and the atmosphere. All these different measurement approaches were adopted to determine the best approach to measure the complex dielectric constant of highly porous bulk materials.

## 3. Results and discussion

For the development and evaluation of the composite regarding its thermal and mechanical behaviour, and behaviour at fire, the amount of PUR that can be added into geopolymer was chosen upon difficulties at preparation and mechanical results of preliminary composites that incorporated a mixture of all used grated PURs.

### 3.1. Determining the optimal amount of PUR inclusion

To ensure the solid workability of MK$_b$, mixing was continued until complete wetting, even though viscosity was not measurable (the viscometer measured torque overload, i.e., the amount of liquid for the used method could not be lowered). However, when the moulded sample was "agitated" a few times, it spread evenly within the mould (the mixture showed thixotropic behaviour, i.e., the amount of liquid did not have to be increased). The maximum amount of PUR$_{mix}$ (mixture of PUR-0, PUR-1, and PUR-2, grated below 1 mm, shown in Fig. 1 c-2 to c-4) included in this study was 5 g, as exceeding this threshold would exceed the workability limit, necessitating additional non-manual force during moulding (the amount of liquid in the mixture was not sufficient). Ultimately, "agitating" the filled mould was not sufficient for the sample containing 5 g of PUR$_{mix}$, which was moulded manually by pressing the fresh mixture into the mould; very similar also for the addition of 4 g. Change in moulding was the reason for the exclusion of the addition of 4 and 5 g of PUR into the MK$_b$ in further study. However, cured composites with such small inclusions did not visually differ from each other (Fig. B1).

For building industry products, compressive strength is usually the most important parameter. Therefore, mechanical strength was evaluated on irradiated and non-irradiated samples with the addition of the grated PUR$_{mix}$ in comparison to the sample without PUR (Fig. 2). As reported in our previous study, compressive strength can increase with irradiation in the early stage of the alkali-activated slurry (Horvat et al.,
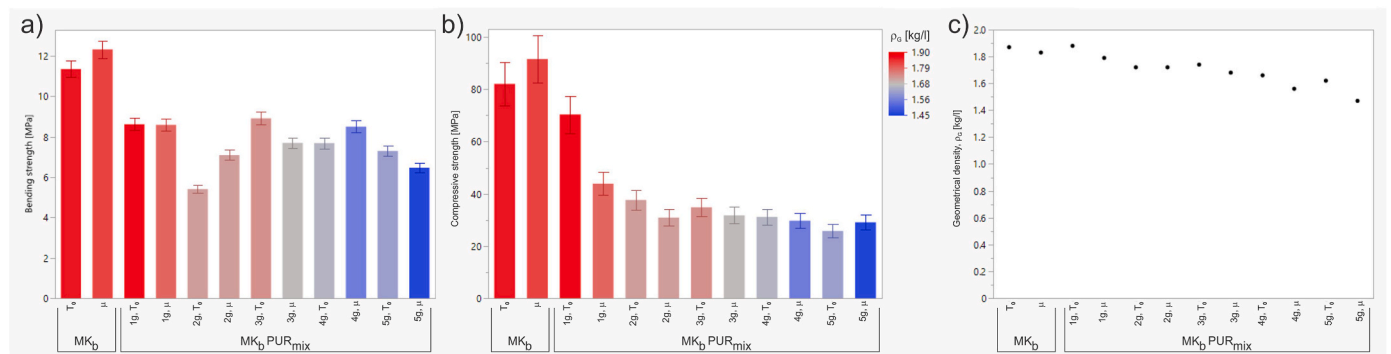
**Fig. 2.** a) Bending and b) compressive strengths (with c) their $\rho_G$) for 14-day-old composite materials containing different masses of grated $PUR_{mix}$ compared to $MK_b$, irradiated with microwaves (μ) and cured solely at room conditions ($T_0$). The biggest standard deviation among samples for bending strength is < 1 MPa (5 % when divided by average value) and for compressive strength is ~15 MPa (~20 % when divided by average value).

2023), which happened with $MK_b$, i.e., sample without PUR. However, the phenomenon reversed for the minimal additions of $PUR_{mix}$ (experiments were repeated once more with the same outcome). Relative changes in the compressive strength because of the irradiation (per addition of $PUR_{mix}$) normalised to non-irradiated counterpart and relative changes because of the addition of $PUR_{mix}$ normalised to $MK_b$ are shown in Table 2. The addition of 2 g of $PUR_{mix}$ resulted in a smaller decrease in the compressive strength because of the irradiation compared to the decrease due to the $PUR_{mix}$ inclusion. The most significant reduction in compressive strength was observed with the inclusion of $PUR_{mix}$, particularly from 1 to 2 g (a 30 % reduction). The addition of 3 g of $PUR_{mix}$ still resulted in a decreased compressive strength value, but the difference was already within the error of compressive strengths (standard deviation) with the sample with added 2 g, as also 4 and 5 g of $PUR_{mix}$. Which excluded the addition of 2 g of PUR in further study.

In this study, several sources could influence the error of compressive strength.

- Heating technique (microwave irradiation):
- The source is a magnetron, which does not offer instant irradiation at the beginning, and every time has a different delay (few seconds) that the operator cannot control, nor measure, but at least the microwave is not in a cyclic mode where microwaves are on on/off without the operator's control,
- The electromagnetic field in the microwave chamber is not uniform, having only a few hot spots where irradiation can have an impact on the material, which was taken into account when positioning the mould/prisms into the microwave, always in the same way to minimize the differences,
- Prisms in the mould, containing the same mixture, could have been filled with slightly different masses (even if the mould was filled to

the top), meaning that some prisms had bigger/smaller potential to be affected by microwave irradiation,
- Prisms in the mould, filled with geopolymer containing PURs, filled to the top, had different masses because of the lower density of the PUR and because PUR used the space where heavier slurry could be, i.e., in samples with PUR there was less water, which is affected by the electromagnetic field. With a bigger amount of PUR replacing slurry in the irradiated prism, this effect should become more obvious and have a bigger impact,
- Physical preparation of geopolymers:
- To minimize human error between samples, only one person was weighting, mixing, moulding, irradiating, and measuring mechanical strengths for all experiments presented in this study,

The moulding procedure for preliminary tests (as described in the Materials and Methods part) was not the same for all mixtures, i.e., mixtures with 4 and 5g of $PUR_{mix}$ had to be (manually) pressed in the mould to get the desired shape, while for all the rest agitation (thixotropic slurry) of the mould was enough. However, the material is not transparent and potential air voids could have remained in the casted slurry, with random location and size. The imperfect manual moulding most likely causes the biggest error of the compressive strength. However, the bending strength did not show a coherent influence on irradiation, as it did on the inclusion of $PUR_{mix}$, regardless of whether or not $PUR_{mix}$ was present in the structure. However, $\rho_G$ logically decreased with the addition of $PUR_{mix}$ (all PURs have lower $\rho_G$, and their addition can only lower $\rho_G$ of the composite). Nonetheless, no exact mathematical conclusions can be drawn because the moulding of samples with 4 and 5 g of added $PUR_{mix}$ was different (additional manual force had to be used). Additionally, irradiated samples showed a slight decrease in $\rho_G$ when compared to their non-irradiated counterparts, which was not expected and because the pattern is obvious for all the samples this can not be a coincidence. The reason behind is not yet understood, however, the current hypothesis is that also PUR itself might have been impacted directly by irradiation (although it has the lowest values of complex dielectric constant among ingredients), as PUR can be found in the literature as microwave absorber when combined with cross-shaped metamaterial absorber (He et al., 2018), and can transmit/scatter different wavelengths of light depending on the PUR aerogel structure and catalyst content (Merillas et al., 2022). How irradiation influences PUR upon prolonged irradiation, like degradation of bonds, changes in density and other properties, has not been reported yet. But its consequence is the decrease in the compressive strength of irradiated samples containing $PUR_{mix}$ (noticeable for smaller additions of $PUR_{mix}$ where the amount of the added $PUR_{mix}$ has a smaller negative influence compared to the irradiation, Table 2).

While a constant play occurs between the negative/positive effects of irradiation and the negative effects of $PUR_{mix}$ inclusion on the

**Table 2**
Relative changes in the compressive strength due to the irradiation (normalisation to the non-irradiated counterpart with the same mass of $PUR_{mix}$) and the addition of $PUR_{mix}$ (non-irradiated samples; normalised to $MK_b$), along with measured values.

| $PUR_{mix}$ addition [g] | 0 | 1 | 2 | 3 | 4 | 5 |
|---|---|---|---|---|---|---|
| Compressive strength, $T_0$ [MPa] | 82.1 | 70.3 | 37.7 | 34.9 | 31.2 | 25.8 |
| Compressive strength, μ [MPa] | 91.6 | 44.0 | 30.9 | 31.8 | 29.7 | 29.12 |
| Irradiation-influenced [%] | 11.6 | −37.5 | −17.9 | −8.9 | −4.6 | 13.0 |
| Influenced by the inclusion of $PUR_{mix}$ [%] | / | −14.3 | −54.1 | −57.5 | −62.0 | −68.6 |

compressive strength, for further evaluation of the influence of the addition of pure PURs, i.e., grated PUR-0, PUR-1, and PUR-2, in the composite, a 3 g PUR was added. This decision was based on the observation that at this level, the detrimental effect of irradiation was outweighed by the negative impact of PUR$_{mix}$ addition. Moreover, the mixing and moulding were still manageable when 3 g were added (when 4 and 5 g of PUR$_{mix}$ was added, moulding needed additional force, but it was still possible to mould the mixture manually; which excluded the addition of more than 3 g of PUR). Because of the desire to add "as much PUR as possible" (to lower $\rho_G$ and $\lambda$, and to use as much waste as possible) lower amounts of PUR additions were not chosen, as also addition of 2 g of PUR$_{mix}$ ended with comparable densities and compressive strengths.

The pore size distribution of the composites containing PUR$_{mix}$ is presented in Fig. 5 a) along with other samples in this study, but were not used for determination of the optimal addition of PUR into the composite. Densities (geometrical, bulk and skeletal) along with total porosities of composites containing PUR$_{mix}$, are presented in Fig. 6 and were not used for determination of the optimal amount of addition of PUR into the MK$_b$ slurry. However, in Fig. 6 b) lower geometrical than bulk density for the addition of 4 and 5 g of PUR$_{mix}$ shows that moulding created inhomogeneity in the sample, which was more prominent for the addition of 5 than 4 g.

To evaluate the reason behind the negative impact of microwave irradiation on compressive strength when a small amount of PUR was introduced into the composite system, the complex dielectric constant of additives (PUR-0, PUR-1, PUR-2, APP and TATA) was measured in the range of 10 MHz to 8 GHz using VNA. Results, shown in Fig. 3 (and Fig. F1), indicate that PURs, APP, and TATA were not completely unaffected by the microwaves of frequency 2.45 GHz, i.e., the real part of the complex dielectric constant ($\varepsilon'$) is above 1 (value for air). This implies that the molecule is not electrically symmetrical (has a permanent electrical dipole) and attempts to align with the outer rapidly-reversing electromagnetic field. This would increase the temperature if the molecules were in a liquid form (not fixed in the solid material) owing to the rubbing with the surrounding molecules. The imaginary part of the complex dielectric constant ($\varepsilon''$) is for PURs zero for the whole measured frequency spectrum; however, for APP and TATA, $\varepsilon''$ increased with frequency. Therefore, their dissipation factor ($\tan\delta = \frac{\varepsilon''}{\varepsilon'}$) also increased. Nonetheless, the dissipation factor of the electromagnetic field, which depends on the material properties, composition and aggregate state (density of the material) (Daminev, 2020), and is mainly caused by anharmonic terms in the potential energy of the crystal and increases by the lattice defects (Tamura, 2006), was for APP and TATA at 2.45 GHz nearly zero, but still significant enough (Tamura, 2006) to be the reason for the non-expected behaviour of the compressive strength owing to low-power microwave irradiation in the early stage of the alkali-activated slurry (both are present in MK$_b$ PUR$_{mix}$). The aggregate state does not change during irradiation, as also does not the composition of the irradiated material. However, its dielectric properties can be

temperature dependent (which was not measured), and APP and TATA are both crystalline (Fig. D2 a)). Besides, APP and TATA went through two chemical experiments: (i) incorporation into PUR-0 during its synthesis, and (ii) incorporation of PUR-0 with APP and TATA (PUR-1 and PUR-2, respectively) along with MK into alkali. Both reactions could have caused the introduction of defects into the crystalline structure of the APP and TATA, which could have enhanced the dielectric loss factor (Tamura, 2006). Nonetheless, APP (and TATA) represents the material in the slurry that is the second (third) most affected by microwaves (after water) according to Fig. 3. While water molecules are evenly distributed in the volume of the mixture, smaller additions of grated PUR "bulk-particles" are not, at least not on the same scale as water molecules. After "rare" PUR particles are heated by microwaves, they become a heat source for their local surrounding area to which they transfer heat conventionally. If the PUR particles are so far apart that this effect stays localized on the macro scale, this might be the source of additional non-uniformity in the prism (microwave heating was performed immediately after moulding and just for 1 min to give a fast temperature "booster" throughout the volume and enhance the dissolution of MK) and cause negative impact to compressive strength. However, the non-uniformity of the initial micro-scale temperature inside the prism can be corrected by adding bigger amounts of less-presented material in the mixture. The change from negative to the positive influence of microwave irradiation on the mixture happened between the 4–5 g of addition of PUR (when moulding had to be performed with additional force; Table 2). However, the noticeable negative impact on compressive strength just by the addition of PUR particles (a heavy non-load carrying material) happened already between 1 and 2 g and it was so severe that no irradiation could fully compensate for the decrease in compressive strength.

### 3.2. Thermomechanical and microstructural evaluation of the selected composites

AAMs exhibit a noncombustible nature, which enables them to safely contain combustible inclusions and offer protection against flames and fire. Therefore, (thermo)mechanical performance (Fig. 4) was evaluated for the samples MK$_b$ and MK$_b$ with the addition of 3 g of PUR-0, PUR-1, PUR-2, i.e., MK$_b$ PUR-0, MK$_b$ PUR-1, MK$_b$ PUR-2, respectively. All samples were treated with low-power microwaves and are shown in Fig. B2, along with samples treated for 2 h at 250, 500, 750 and 1000 °C.

Compressive strength results (Fig. 4b–Table 3) for samples treated with microwaves but not exposed to elevated temperatures indicated a high influence of the addition of different PURs (Table 3). However, all three PURs were tested in our previous study (Mušič et al., 2022) and showed similar low compressive strength, where PUR-1 reached approximately two-thirds of the compressive strength of PUR-0 and PUR-2. Therefore, the additional lowering of compressive strength of the composites containing PUR-1 (contains APP) and PUR-2 (contains TATA) could be due to the irradiation. To exclude the potential negative influence of chemical reaction between alkali and APP/TATA,
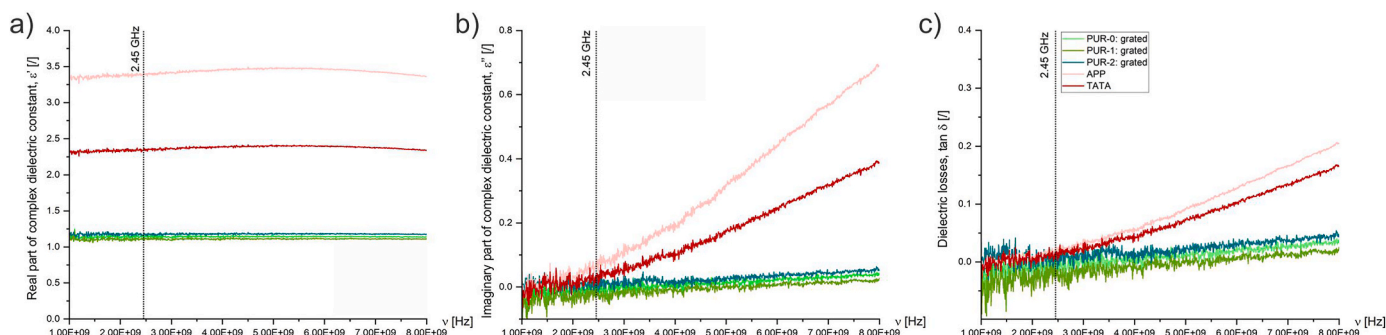


**Fig. 3.** Complex dielectric constant ($\varepsilon' + i \bullet \varepsilon''$) and losses ($\tan\delta$) in dependence of the frequency for powders APP and TATA, and grated PUR-0, PUR-1, and PUR-2.
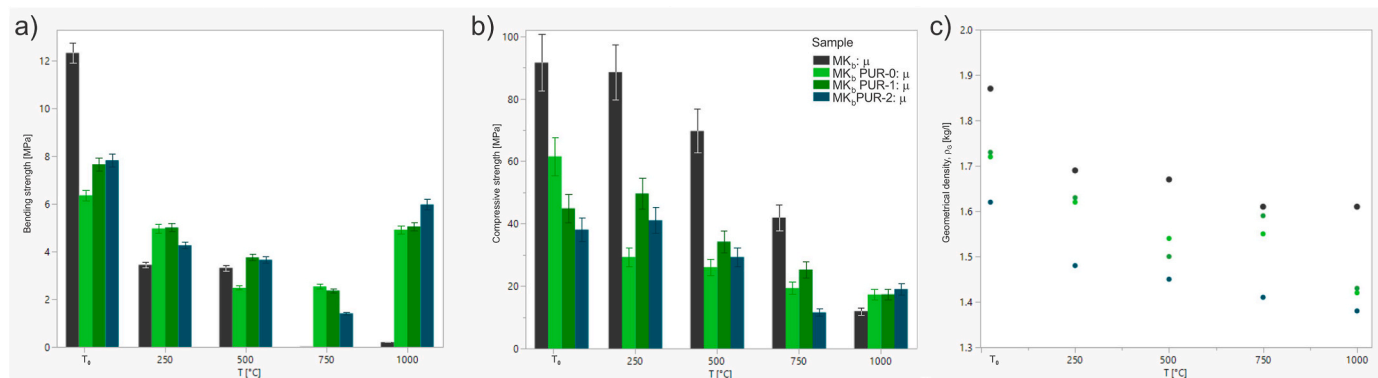
**Fig. 4.** Temperature dependence of a) bending and b) compressive strength and c) $\rho_G$ of the 14-day-old composite samples. The biggest standard deviation among samples for bending strength is $< 1$ MPa (5 % when divided by average value), and for compressive strength is $\sim 15$ MPa ($\sim 20$ % when divided by average value).

geopolymer composites using MK and alkali (both were used also in present study) with the inclusion of APP or TATA (no PUR) were synthesized and reported in our previous study: (i) APP reacted with alkali, which lead to a severely low mechanical performance, (ii) TATA just got incorporated into the ASN without any reaction with other ingredients (Mušič et al., 2023b). However, when both flame retardants are part of the PUR, the geopolymer composite with APP shows better mechanical performance than the geopolymer composite with TATA. Therefore, geopolymer only embedded PURs, irrespective of their flame retardants content. Another possibility of reduced mechanical performance of composites containing PUR-1 and PUR-2 would be their different porous structure (Fig. 1 b), but this was ruled out by grating the samples (Fig. 1 c-2 to c-4). In addition, their lower $\rho_S$ compared to PUR-0 (Fig. 6 b, data are also in the Materials and methods) exerted no coherent effect on composite's $\rho_G$ (Fig. 4 c).

In general, the compressive strength of all samples decreased with temperature. However, unexpectedly, all composites initially containing PURs exhibited higher compressive strength than $MK_b$ when exposed to 1000 °C (although having lower $\rho_G$), which is due to the more prominent cracks in sample $MK_b$ that were not detected using MIP (maximum upper limit = 1 mm) or SEM (cracks are too big even for lower SEM magnifications) (Fig. B2 a, 1000 °C), and cause bigger mechanical strength problems than if sample would have a lot of smaller pores.

Like compressive strength shows negative impact on increase in temperature, so does bending strength, at least up to 750 °C. However, because bending strength is not enhanced with any fibrous material, it is several times lower compared to compressive strength with or without PUR. However, bending strength for samples that initially contained PUR was at 1000 °C much higher. The reason behind is the same as for the compressive strength, i.e., formation of large prominent cracks in $MK_b$. While there were cracks also in case of composites initially containing PURs at 1000 °C (Fig. B2 b-d), bending strengths were higher than bending strengths at 250 °C, although $\rho_G$ (Fig. 4 c) decreased. The decrease of $\rho_G$ means that cracks od/and pores formed in the sample (which can be seen in SEM micrographs in Fig. 7 e), but if there would not be any "enhancement" of the skeleton of the material, bending strength would have lowered too. This leads to the conclusion, that $\rho_S$ increased (which was confirmed by MIP, see Fig. 6).

The evolution of porosimetry enables the assessment of the severity of the impact of prechosen parameters on the material, including how well an additive fills the pores or introduces additional ones or how the pore-size distribution changes owing to the heat treatment. The addition of different amounts of $PUR_{mix}$ into the system (Fig. 5 a) did not impact the pore-size distribution. Any observed differences in the distribution are attributed to the moulding process (for 4 and 5 g additional force was needed for moulding, as described in the chapter for determination of optimal amount of PUR inclusion) and selection of a smaller portion (ranging from 1 to 2 g from the entire prism; rough choice of mass of the

sample depends on the stem volume of the used penetrometer and on the predicted total porosity of the sample) of the composite for MIP measurement. Similarly, total porosity (Fig. 6 a) was not influenced by adding $PUR_{mix}$, or irradiation. If irradiation would be performed at higher powers (1000 W), geopolymers would foam, but at 100 W no increase of porosity was expected (Horvat et al., 2023). Therefore, alkali-activated slurry effectively filled all the corners in the grated $PUR_{mix}$, and no additional pores were created by adding grated $PUR_{mix}$ (quality of encapsulation can be seen in Fig. 7 a and Fig. C1 a). When comparing the total porosity of PUR-0, PUR-1, and PUR-2 (Fig. 6 a) to the total porosity of composites, the porosity of the composites is the porosity of the $MK_b$, as $MK_b$ also represents the majority of the composite.

However, the inclusion of 3 g of PUR-0, PUR-1, or PUR-2 into the geopolymer, in comparison to $MK_b$ (all samples were treated with microwaves), lowered the number of pores from 0.1 to 1 μm (decrease of the corresponding peak with peak at 0.3 μm in Fig. 5 b) but also increased the number of smaller pores (increase of the peaks left to the sharpest peak for $MK_b$, at 0.3 μm; i.e., increase of the peaks at 0.01 and 0.02 μm Fig. 6 b)). While the addition of PUR-0 maintained the tri-modal pore-size distribution with three prominent Gaussian peaks (with peaks at 0.005, 0.04 and 0.2 μm), the addition of PUR-1 resulted in only two prominent Gaussian peaks (with peaks at 0.006 and 0.02 μm), and the composite with PUR-2 resulted in only one prominent peak at 0.007 μm.

For all irradiated samples ($MK_b$, $MK_b$ PUR-0, $MK_b$ PUR-1, and $MK_b$ PUR-2), exposure to elevated temperatures, 500 °C and higher, altered the pore-size distribution, i.e., the higher the temperature, the bigger the pores (Fig. 5 c–f) and higher total porosity (Fig. 6 a).

While the addition of $PUR_{mix}$ (1–5 g, where 5 g of PUR is only 7 m% of the whole composite without water) did not significantly influence $\rho_S$ and $\rho_B$ of the composites (compared to $MK_b$; all samples were held at 70° until MIP measurement), Fig. 6 b, 14-day-old $\rho_G$ (measured just before mechanical strength evaluation without additional drying to the constant mass) showed a negative trend upon the addition of the increasing amount of $PUR_{mix}$. While $\rho_G$ and $\rho_B$ often have similar trends, if not values, higher $\rho_G$ than $\rho_B$ (unless error was made by measuring $\rho_G$ or if not well representative part of the sample was selected for MIP measurement) can be attributed to the presence of water in the structure (water increases the mass of the sample; water was detected by FTIR in all 14-day-old composites, Fig. D1), while smaller $\rho_G$ than $\rho_B$ can be attributed to large open pores/cracks/cavities/voids for MIP to detect them and inhomogeneity of the bulk material (large cracks can be seen in $MK_b$ sample treated at 1000 °C in Fig. B2 a). Because the fresh mixture had to be irradiated immediately after moulding (this procedure usually takes up to 2 min), the inhomogeneity in the composite with higher amounts (5 g) of added $PUR_{mix}$ is possible owing to the poor workability of the slurry.

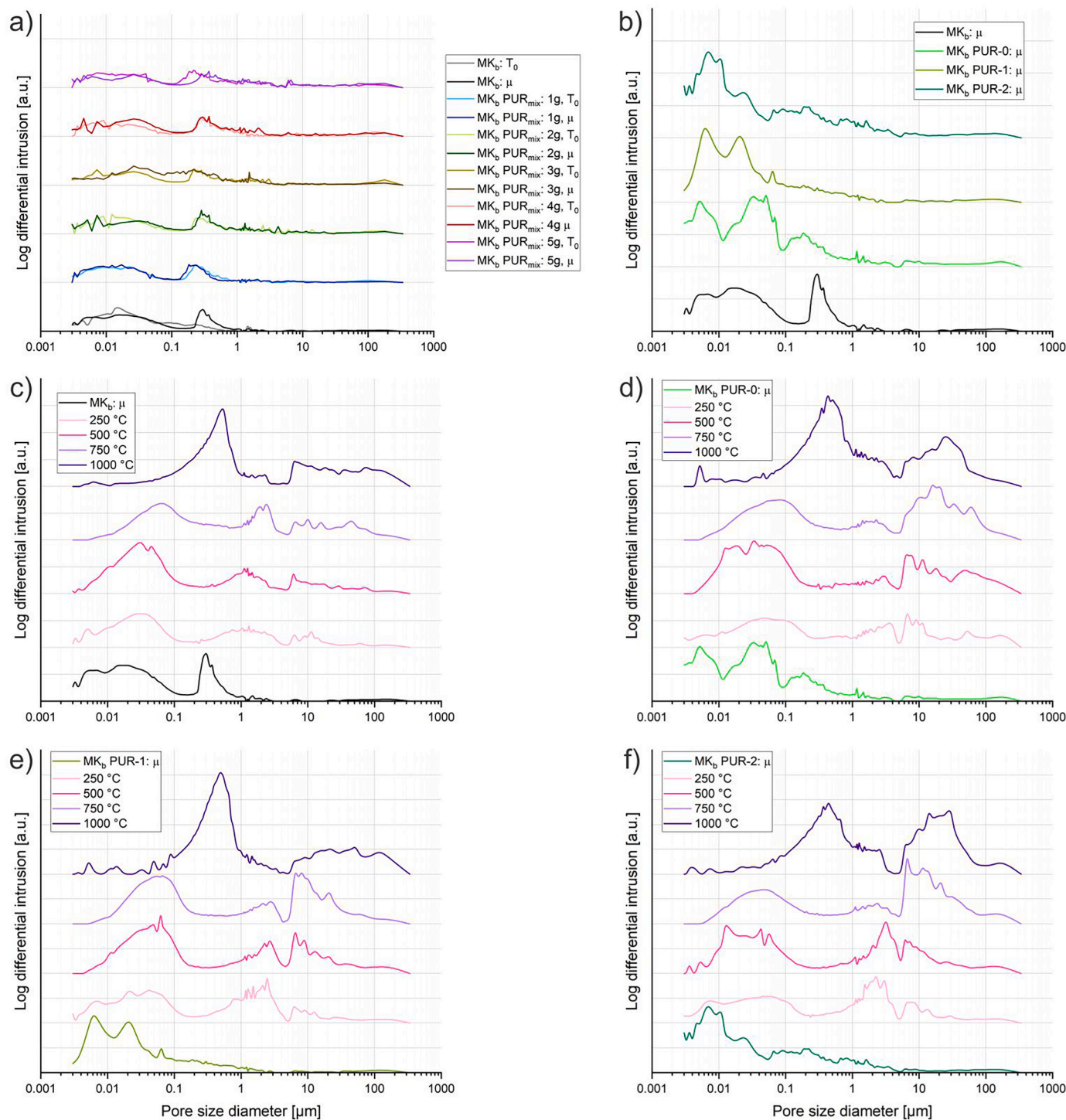Nonetheless, the trend of lowering the $\rho_G$ of the composite material,

**Fig. 5.** MIP pore size distribution for composite samples made from a) $PUR_{mix}$ (1–5 g) and b-f) PUR-0, PUR-1, PUR-2 (3 g) in comparison to geopolymer without PUR (black and grey), untreated and treated with microwaves ($T_0$ and $\mu$, respectively). c-f) MIP pore size distribution for irradiated composites with pure PURs compared to $MK_b$ at elevated temperatures.

when a material with a much smaller density is added, is valid (if no chemical reaction occurs between the materials). Because PURs integrated into geopolymer composites are grated (the structure is destroyed, pores conferring lower $\rho_B$ and $\rho_G$ to the PUR are absent, Fig. 1 c-2 to c-4), its contributing density in the composite is (mainly) skeletal (Fig. 6 b), as can be seen in Table 4a-c (the formula used for calculations is in appendix Eq. (E.1), as are the graphs for all four combinations for each PUR in Fig. E1; the Excel file for the calculation of the composite density is in the Supplement, where mass of added PURs can be changed

without restrictions). Namely, the 14-day-old measured $\rho_G$ (bold black values in Table 4a) can be compared to the calculated $\rho_G$ where inclusions contribute with their $\rho_S$ (blue bolded values in Table 4b). Notably, at 14 d, the samples retain a certain amount of water. Therefore, the calculations are also conducted on the entire slurry (and not just on solid material), providing the maximum possible value for density.

In Table 4b is presented calculated $\rho_G$, when the mass of added PUR is 3 g (like in this study), and in Table 4c is calculated $\rho_G$ when the mass
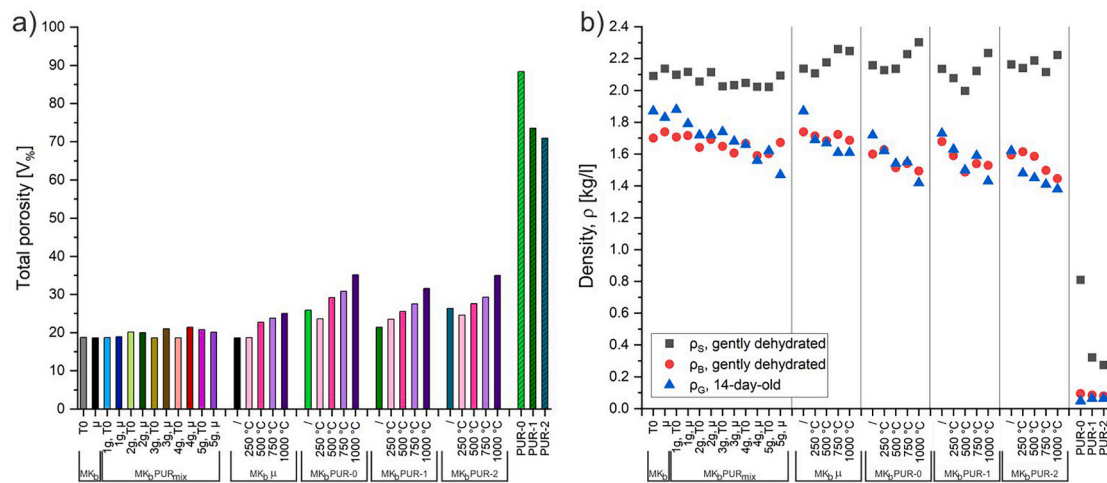
**Fig. 6.** MIP results (stem volume was from 26 % to 83 %) for all composites compared to geopolymer without PUR and PUR (PUR-0, PUR-1, PUR-2): a) total porosity, b) $\rho_S$ and $\rho_B$ in comparison to $\rho_G$.

**Table 3**
Compressive strength values at room conditions and elevated temperatures, and their relative changes for irradiated MK$_b$ PUR-0, MK$_b$ PUR-1 and MK$_b$ PUR-2 normalised to MK$_b$, at room conditions.

| Composite | MK$_b$ | MK$_b$ PUR-0 | MK$_b$ PUR-1 | MK$_b$ PUR-2 |
|---|---|---|---|---|
| Compressive strength at $T_0$, μ [MPa] | 91.6 | 61.6 | 44.9 | 38.1 |
| Compressive strength at 250 °C, μ [MPa] | 88.5 | 29.3 | 49.7 | 41.1 |
| Compressive strength at 500 °C, μ [MPa] | 69.7 | 26.1 | 34.3 | 29.3 |
| Compressive strength at 750 °C, μ [MPa] | 41.9 | 19.4 | 25.3 | 11.6 |
| Compressive strength at 1000 °C, μ [MPa] | 11.9 | 17.3 | 17.4 | 19.0 |
| Influenced by type of PUR [%] | / | −32.7 | −50.9 | −58.4 |

of added PUR is 50 g (equal to the mass of MK in the mixture). The last mixture in this study is experimentally not possible (it was performed just for theoretical comparison).

Therefore, as predicted from Fig. 1 c-2 to c-4, PUR inclusion does not lower $\rho_G$ of the composite with its structure (skeleton and pores) but just with the skeleton itself: the density of the material is higher than that of the porous structure made from the same material (Fig. 6 b). This implies that the density of the final composite is not controlled only by the mass of added PUR, but also by the grating quality. Namely, if the grated PUR retains the porous structure, which is not filled with geopolymer but with air/gas (to keep the density low), and is uniformly distributed in the composite, it can lower $\rho_G$ of the composite better than the well-grated material where the porous structure with its extrinsic properties is destroyed and only intrinsic properties remain (Fig. 1 c-2 to c-4). As can be seen in Table 4b-c, when comparing double-underlined cells for composite containing PUR-0, the addition of 3 g (like in this study) of poorly-grated PUR confers to $\rho_G$ of the composite material <0.8 kg/l, but if the PUR is well-grated (like in this study) and its amount is the same as the amount of MK (50 g, i.e., the mass of PUR would be > 15 times than it was used in this study), the $\rho_G$ of the composite is > 1.2 kg/l. However, if the density of the composites is lowered with not the lowest possible density of the inclusion material (when the quality of grating of PUR is between perfect destruction and complete retention of the porous structure, and all up to the well-grated PUR), adding 5 g of PUR$_{mix}$ could not result in the $\rho_B$ of the composite being as high as if there were no PUR in the composite, that occurred in this study. The same is true for

the $\rho_S$ (Fig. 6 b). Therefore, the irradiated composite with 5 g of PUR$_{mix}$ was indeed inhomogeneous (affecting all the properties of the composite), and it is not appropriate for any kind of upscaling owing to inhomogeneity caused by tough preparation. Hence, it is impossible to produce the theoretical mixture shown Table 4c, where 50 g of PUR was added (the dark grey part of the table). Nonetheless, MIP has the potential to be used as a tool for the determination of millimetre-scale (in) homogeneity of the samples when compared to their cm-size comparable values if the measurements are done in the reliable stem volume span, the penetrometer's metal envelope is intact and all accompanying measurements of the samples are performed correctly.

With the thermal treatment of MK$_b$ and composites including PURs, $\rho_B$ and $\rho_G$, it generally decreased. At 250 °C, no water was left in the material (according to FTIR in Fig. D1), which lowered $\rho_G$ just by the decrease of the mass due to the evaporation, besides the potential creation of cracks that are used as evaporation paths in fuller structures. At 250 °C, the organic inclusions in the geopolymer resulted in damages (Fig. 7 b). This led to a small decrease in the mass, but also contributed to lowering the densities. At 500 °C, no PURs were left in the composites, leading to the additional decrease in $\rho_G$, and at 1000 °C, deterioration of the ASN (Fig. 7 e) showed its impact on both densities. The rate of the decrease in $\rho_G$ and $\rho_B$ is lowest for MK$_b$, which has no thermally weak inclusions.

Although the total porosity increased with temperature (Fig. 6 a), which lowered $\rho_G$ of the material, $\rho_S$ (Fig. 6 b) remained the same or increased owing to the inner pressure of released gasses onto the remaining structure from all sides and due to the formation of minerals. As seen in Fig. D2, not many different minerals were present in the inorganic part of the composites, just quartz, which is already present in the precursor and remains present in the composite also at 1000 °C. While nepheline formed at 1000 °C in all samples, and contributed to the ratio mineral towards amorphous material. Amorphous material is in general softer than ordered structures (crystalline material), which have atoms packed in denser structures (Yue, 2022), which is the reason for the increase in the $\rho_S$ of the composite at 1000 °C. However, for MK$_b$ PUR-1, $\rho_S$ was decreasing up to 500 °C, which can be due to the reactions of acidic compounds with alkali ASN (as seen in the SEM micrograph in Figs. 7 b-3). When the acidic negative effect was absent, $\rho_S$ increased.

The thermal behaviour of the composites was studied using SEM (Fig. 7), focusing on organic inclusions and changes in the ASN (micrographs depicting SEM statistical data, cracks, and pores are shown in Fig. C1). At room conditions (Fig. 7 a), all PURs were well embodied in the geopolymer, and no notable differences are observed in the ASN of all samples. Although the incorporated PUR was well embedded in the
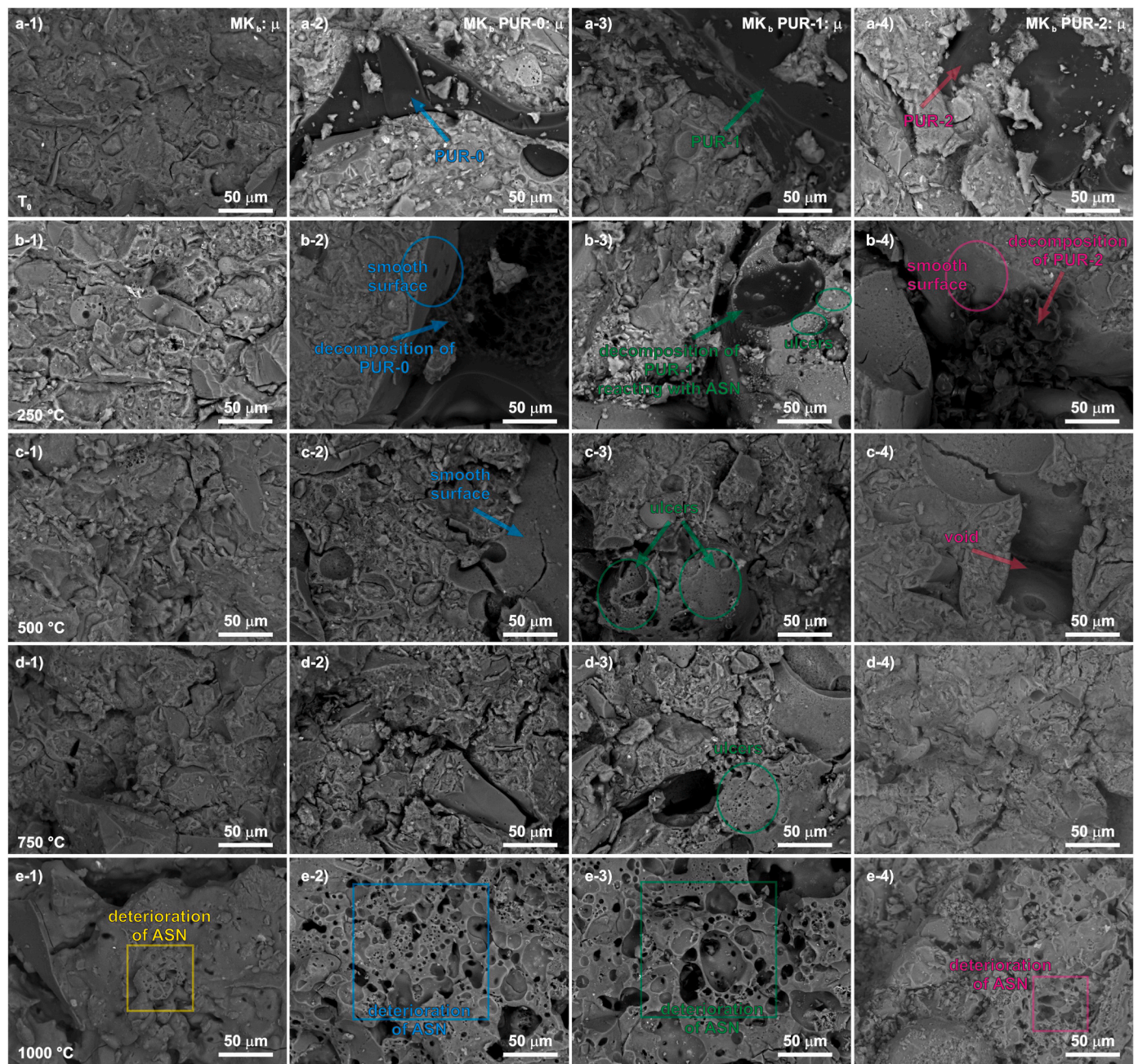
**Fig. 7.** SEM micrographs (500-times magnified) of 1) geopolymer MK$_b$ and composites with incorporated 2) PUR-0, 3) PUR-1, and 4) PUR-2 treated at selected temperatures (a) room conditions, b) 250 °C, c) 500 °C, d) 750 °C and e) 1000 °C).

**Table 4.a**

Measured $\rho_G$ and $\rho_S$ of the irradiated composites (MK$_b$ PUR-0, MK$_b$ PUR-1 and MK$_b$ PUR-2) and of the PUR-0, PUR-1 and PUR-2. Text in grey is data not used in the calculations in Eq. (E.1).

| Sample | MK$_b$ | MK$_b$ PUR-0 | MK$_b$ PUR-1 | MK$_b$ PUR-2 | PUR-0 | PUR-1 | PUR-2 |
|---|---|---|---|---|---|---|---|
| $\rho_G$ [kg/l] | 1.83 | **1.72** | **1.73** | **1.62** | 0.05 | 0.06 | 0.06 |
| $\rho_S$ [kg/l] | 2.14 | 2.16 | 2.14 | 2.16 | 0.81 | 0.32 | 0.27 |

geopolymer (bulk PUR-0 in geopolymer is shown in Supplement 2 in Fig. S2), there we re still gaps between the PUR-geopolymer boundary found (SEM micrographs are in Supplement 2 in Fig. S3). However, eve n

if there are no chemical bonds between PUR and ASN, grated PUR is of random curved shapes (Fig. 1 c-2 to c-4) and ASN around it immobilizes it physically. Nonetheless, the composite with APP seemed to have on the surface of PUR-1 well-attached geopolymer (side surface of the PUR-1 in Supplement 2 in Fig. S3 d-2). Although no visible differences are observed among PU R-0, PUR-1, and PUR-2 at room conditions, at 250 °C they all showed signs of "ongoing" decomposition, with notable differences, particularly for samples containing PUR-1. PUR-1 contains APP, which is a source of acidic compounds when exposed to elevated temperatures (decomposition starts up to 300 °C, depending on the length of the chain of the molecule) (Fan and Fu, 2017). Because geopolymer is alkaline, a combination of decomposing APP and alkaline ASN forms circular/half-spherical ulcers on the surface of the ASN (which was in contact with degrading PUR-1, Figs. 7 b-3, green circles). These ulcers are visible for MK$_b$ PUR-1 also at higher temperatures

**Table 4.b**
Calculated $\rho_G$ of the irradiated composites (MK$_b$ PUR-0, MK$_b$ PUR-1 and MK$_b$ PUR-2) using Eq. (E.1) and experimental data (mass of PUR is 3 g). Text in blue are calculated $\rho_G$ of composites when inclusions contribute to the $\rho_G$ of the composite with their $\rho_S$, and in green when their contribution comes from their $\rho_G$.).

| | Calculated on | MK$_b$ PUR-0 | MK$_b$ PUR-1 | MK$_b$ PUR-2 | The density of PUR in the composite |
|---|---|---|---|---|---|
| $\rho_G$ [kg/l] | Slurry | **1.75** | **1.57** | **1.53** | $\rho_S$ |
| | Solid | **1.73** | **1.51** | **1.46** | |
| $\rho_G$ [kg/l] | Slurry | 0.78 | 0.93 | 0.93 | $\rho_G$ |
| | Solid | 0.68 | 0.82 | 0.82 | |

**Table 4.c**
Calculated $\rho_G$ of the irradiated composites (MK$_b$ PUR-0, MK$_b$ PUR-1 and MK$_b$ PUR-2) using Eq. (E.1) and experimental data (mass of PUR is equal to mass of MK, i.e., 50 g). Text in blue are calculated $\rho_G$ of composites when inclusions contribute to the $\rho_G$ of the composite with their $\rho_S$, and in green when their contribution comes from their $\rho_G$.) Mixture with the amount of alkali used is not possible, but it was not changed for the comparison reasons.

| | Calculated on | MK$_b$ PUR-0 | MK$_b$ PUR-1 | MK$_b$ PUR-2 | The density of PUR in the composite |
|---|---|---|---|---|---|
| $\rho_G$ [kg/l] | Slurry | 1.24 | 0.66 | 0.58 | $\rho_S$ |
| | Solid | 1.18 | 0.60 | 0.53 | |
| $\rho_G$ [kg/l] | Slurry | 0.12 | 0.16 | 0.16 | $\rho_G$ |
| | Solid | 0.10 | 0.14 | 0.14 | |

(green circle in Fig. 7).

At 500 °C, no organic material remained, a fact corroborated by FTIR analysis (Fig. D1). Instead, only voids with smooth surfaces (and ulcers in the case of MK$_b$ PUR-1) were observed, where PURs had been in contact with ASN (Fig. 7 c). No additional changes were observed at 750 °C, as confirmed by SEM, FTIR, and XRD analysis (Fig. D2). However, at 1000 °C, deterioration of the ASN was evident throughout the composites containing PURs, while MK$_b$ shows only the start of the deterioration (Fig. 7 e; yellow square). In addition, mineralogical changes (according to XRD) occur with comparable intensities at this temperature, regardless of the initial inclusion of PUR (Fig. D2). Because deterioration of ASN at 1000 °C is for MK$_b$ minimal (yellow square in Figs. 7 e−1), while for all other composites containing PUR is present everywhere over the observed SEM area, deterioration of ASN is not connected with mineralogical changes.

### 3.3. Thermal and fire-behaviour evaluation of the selected composites

In addition to the fact that the inclusion of PURs in MK$_b$ (Fig. 8 c) affected $\rho_G$ of the composites (Figs. 6b–Fig. 8 b, Table 5) solely by the $\rho_S$ of PUR, it also affected $\lambda$ of the composites (Fig. 8 a and Table 5) which depend on the material (skeletal; the influence of the "chemistry") and material's structure (porosity, $\rho_G$; the influence of the "physics"). Although the material from which the skeleton of the composite is made is important in thermal insulation, a far bigger benefit in insulation is its open/closed porosity. Therefore, the inclusion of poorly grated PUR,

**Table 5**
Changes in the thermal properties and $\rho_G$ of irradiated geopolymer because of the addition of 3 g of PUR-0, PUR-1, and PUR-2, calculated on MK$_b$ as the difference to MK$_b$.

| Composite | MK$_b$ | MK$_b$ PUR-0 | MK$_b$ PUR-1 | MK$_b$ PUR-2 |
|---|---|---|---|---|
| $\lambda$ [mW/(m·K)] | 942 | 884 | 867 | 856 |
| $\rho_G$ [kg/l] | 1.83 | 1.72 | 1.73 | 1.62 |
| $\lambda$ [%] | / | −6.2 | −8.0 | −9.1 |
| $\rho_G$ [%] | / | −6.0 | −5.5 | −11.5 |

which, with its porous nature and captured air, would additionally lower the density with its much lower $\rho_G$ than $\rho_S$ (Fig E1), would positively impact $\lambda$ of the composite.

The decrease in $\lambda$, as can be seen in Tables 5 and is biggest when PUR-2 was used as the inclusion in the composite (from 942 to 856 mW/(m·K)), which also had biggest decrease in the density (from 1.83 to 1.62 kg/l). If the density would be lowered obeying Fig. E1, $\lambda$ would follow its decrease.

However, the porous "chunks" of poorly grated PUR would represent much bigger amounts of fire fuel with easily accessible air from their pore system, and their maximum addition into geopolymer would be limited by their fire-behaviour response, which is shown for tested composites (MK$_b$ PUR-0, MK$_b$ PUR-1, MK$_b$ PUR-2) in Fig. 9. Fire-results are compared to MK, MK$_b$ and PUR-0, PUR-1 and PUR-2, once factorised to the equal mass of "composite" material (to the mass of MK$_b$; Fig. 9, columns 2 and 3) and once to the equal amount of the fuel (10 g, in Fig. 9
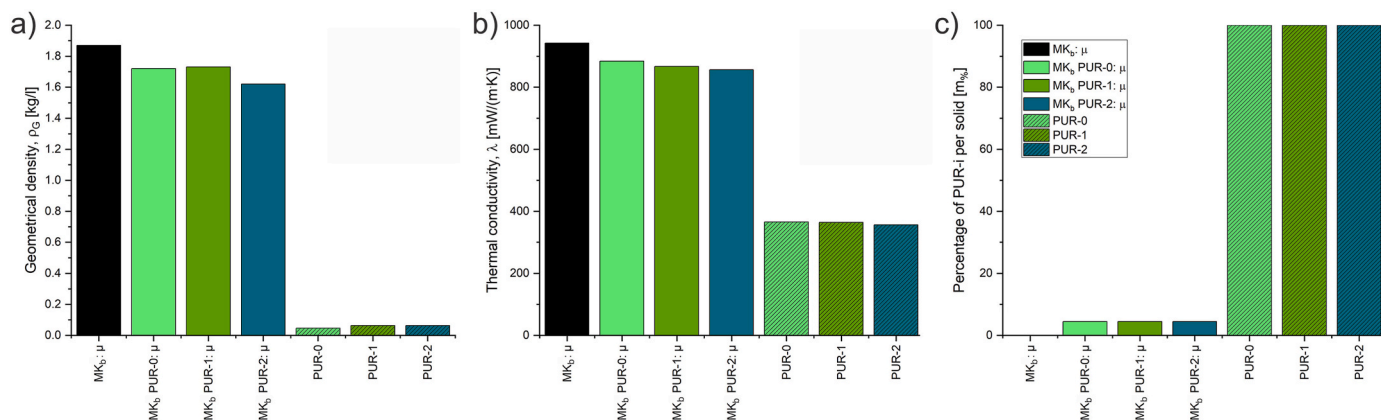


**Fig. 8.** (a) $\lambda$, (b) $\rho_G$, and (c) mass percentage of PUR in the composite for: irradiated geopolymer composites MK$_b$, MK$_b$ PUR-0, MK$_b$ PUR-1, MK$_b$ PUR-2, and non-irradiated PURs PUR-0, PUR-1, PUR-2. The thermal properties of PURs were reported in our previous study (Mušič et al., 2022).
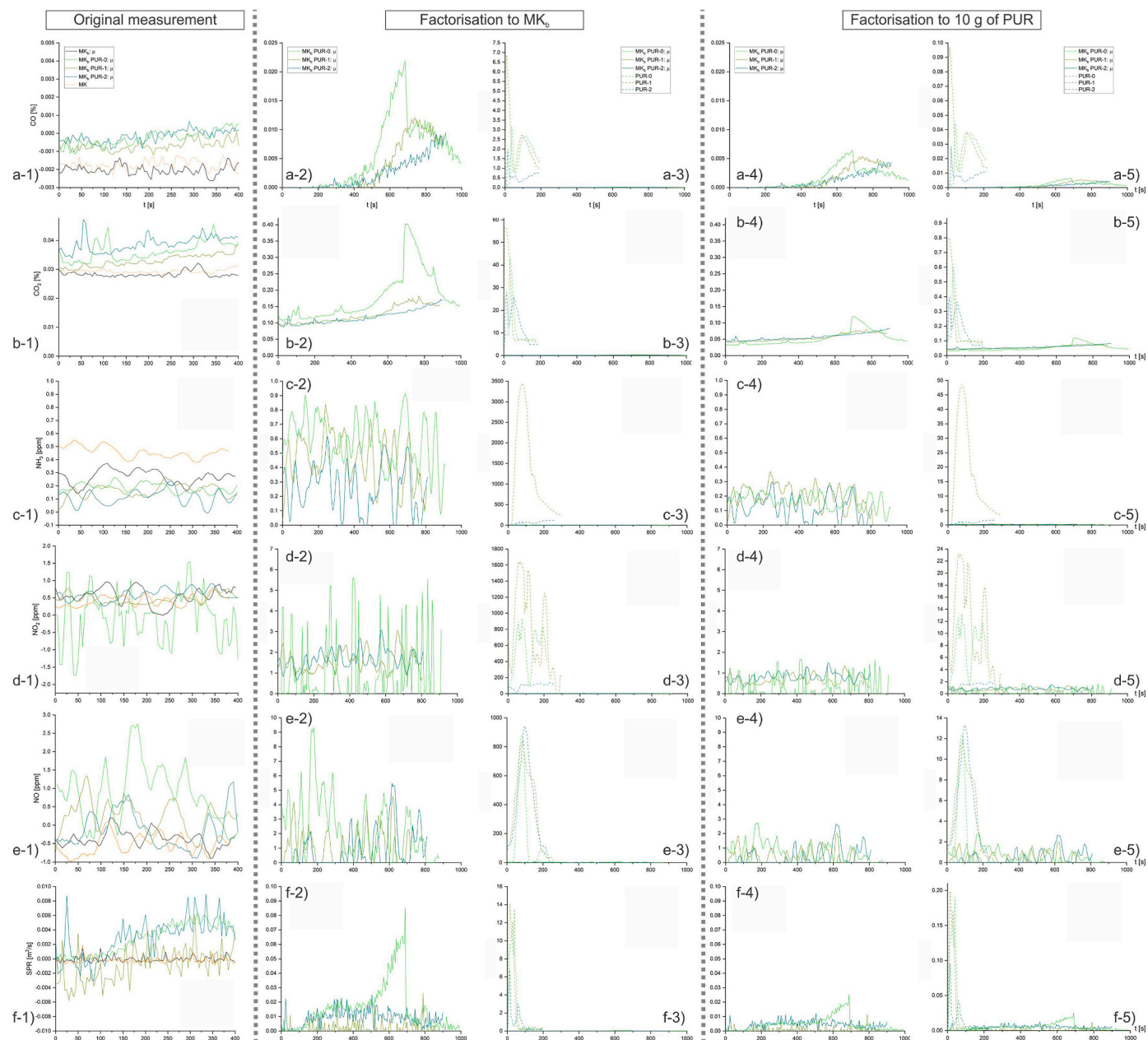
**Fig. 9.** 1) Cone calorimeter (CO, CO$_2$, SPR) and atomsFTIR measurements (NH$_3$, NO, NO$_2$) for MK and MK$_b$, and for composites MKb PUR-0, MKb PUR-1, MKb PUR-2, compared to PUR-0, PUR-1 and PUR-2. 2 and 3 are factorised measurements to the largest tested mass (MK$_b$), 4 and 5 to the same mass (10 g) of "fire fuel" (PUR).

columns 4 and 5), using formulas Eq. A.1, Eq. A.2 and Eq. A.3. Unaltered measurements are shown in Fig. 9, column 1, while measurements for PURs were provided in our previous study (Mušič et al., 2023b).

Smoke production (smoke production rate, SPR) for all PURs (their mass was about 5 g) (Mušič et al., 2022), with and without flame retardants (APP and TATA), started very early and intensively after being exposed to only 40 kW/m$^2$ of heat flux, and self-ignited around 10 s (PUR-1 and PUR-2) or 30 s (PUR-0) after being exposed to heat. Flame duration in the case of PUR-0 was 2–3 times shorter when compared to PURs containing flame retardants but was much more intensive. However, all PUR reactions with fire ended 1–2.5 min after the exposure to a heat source started. In the case of the composites containing PURs (mass >300 g), embedded in a noncombustible MK$_b$ (black line in Figs. 9 f-1) made from a noncombustible MK (orange line in Figs. 9 f-1), exposed to the heat flux 50 kW/m$^2$, after 4 min hardly reached SPR value of PURs when the reaction to fire ended. After 500 s of exposure to the heat flux,

MK$_b$ PUR-0, which is the only composite that does not contain any flame retardant, showed a SPR peak (Figs. 9 f-2, which coincides with detecting CO and CO$_2$ gasses (Fig. 9 a-2 to a-5 and Fig. 9 b-2 to b-5, respectively). For composites containing flame retardants AAP or TATA in PUR, the SPR value never showed any peak. Nonetheless, among gasses, that help to put the fire down (Fig. 9 a–e), only CO and CO$_2$ were detected for composites containing PUR with flame retardants. However, when compared to PUR-0, PUR-1, and PUR-2, the CO and CO$_2$ values of the composites were negligible when the values were factorised to equal mass (MK$_b$; Fig. 9 column 3) or to equal mass of fuel (10 g; Fig. 9 column 5). Only the release of CO and CO$_2$ and SPR values for MK$_b$ PUR-0, when factorised to the same fuel mass (PUR), were above the noise. Therefore, well-grated and well-encapsulated PUR in a non-combustible material does not hinder the combustion of PUR, but it changes its combustion into controlled combustion with much lesser fire hazard to the environment.

## 3.4. Current limitations of the proposed approach

The proposed approach of incorporating grated PUR with or without flame retardants into geopolymer for use in building insulation presents several promising aspects but also has certain limitations. Among other things, the approach deals with the problem of waste management by using waste PUR materials, thereby reducing the impact on the environment associated with the disposal of these materials. Here, it is necessary to mention the limitations in the use of waste, which arise in the question of their history (exact preparation/composition of PUR waste, e.g. exposure to UV, rain, elevated temperatures, etc.). This part should be discussed/researched separately in more detail by incorporation of PURs synthesized with different molar ratios between isocyanates and polyols, and aged with different parameters.

Incorporating grated PUR into the geopolymer reduces the density of the composite material, which can be beneficial for applications such as building insulation where lightweight materials are desired and also improves the thermal insulation of the geopolymer, which can contribute to improved energy efficiency in buildings, but on the other hand, degrades the mechanical properties of the geopolymer and additional tests are required before their use for a specific purpose (where the properties of the new composite are evaluated regarding the application requirements). Mechanical properties can be a significant limitation, especially in applications where structural integrity and load-bearing capacity are critical. Therefore, to be able to choose the final mixture reversely, i.e., according to the final product (minimal) requirements, mechanical and thermal properties should be evaluated also for composites where PUR does not have destroyed porosity, and for composites containing a known ratio of PUR from both "fractions", to create parallel 2D-maps to the "map" of the geometrical density of the composite (Fig. E1).

While flame retardants (APP and TATA) are introduced to address the flammability of pure PUR, the study finds that the flammability of grated PUR, even without flame retardants, becomes more hindered when incorporated into geopolymer. To keep composite fire-safe, different sizes of PUR with non-destroyed porosity should be tested with different ratios of geopolymer, to evaluate the minimal thickness of the walls between different PUR particles which can prevent the localized flames during the combustion of PUR from joining into the fire. This should be one of the parameters taken into account during the synthesis of the composite of desired final thermal/mechanical properties.

To be able to easily incorporate more PUR into the slurry, the needed minimal addition of water should be evaluated in connection with the surface area of added PUR that gets into contact with the slurry. At the same time, the viscosity (or slump cone test) should be maintained, if the initial alkali-activated mixture was already optimal. However, the mechanical performance of such prepared composites should be compared to composites without the extra addition of water and taken into account regarding the desired properties of the final composite.

This study also mentions using microwaves at low power to address the potential loss of mechanical efficiency due to PUR incorporation. Namely, the positive influence of microwaves on composites was expected because microwaves had a positive influence on geopolymer itself. However, there was a negative impact on compressive strength not just due to the addition of PUR, but also because of the irradiation with microwaves when the addition of PUR was lower. At this moment the

hypothesis is that microwaves also affect PUR, and if PUR particles are too far apart that this effect is localized to a few areas, additional non-uniformity is introduced into the composite. Besides, if PUR absorbs microwaves, there are less "microwaves" available for heating water, if the spread of the heat from the solid PUR is not as efficient as from small liquid water molecules. Therefore, the scattering/transmittance/absorption of microwaves on PUR itself has to be evaluated separately.

## 3.5. Prospects of the proposed approach

In the scope of reduction of waste, use of raw materials and pure chemical substances, and with the aim for sustainability in the building and civil engineering sector, composites of geopolymer with embedded grated (flammable, low density and low thermal conductivity) waste PUR were prepared and the potential to design fire-safe(r) composite, where mechanical and thermal properties are linked with its (micro) structure, was shown. To further reduce the weight and thermal conductivity of the composite, more PUR should be incorporated into the geopolymer, which means that the liquid part of the slurry should be increased with regards to the minimal required mechanical properties (and maintaining the fire-safety) for the building and civil engineering product in design. Compared to chemical foaming of the geopolymers, incorporation of the lightweight "aggregates" (like PUR) is much more worker-friendly due to the reduction of the use of hazardous chemicals that are needed for chemical foaming (foaming and stabilizing agents (Horvat and Ducman, 2019)) and represent a viable option for upscaling onto the industrial level.

There are several additional benefits of using waste PUR in the geopolymer for weight and thermal conductivity decrease, and for using geopolymer to embed flammable waste PUR.

- Energy reduction: to produce polyurethane and geopolymers, it is necessary to supply energy (in the form of heat). If 5–15 % of waste PUR can be added to geopolymer, it means that in the production of geopolymers, 5–15 % of the energy needed for the production of raw materials (pure PUR) is saved. It is also necessary to mention that our new PUR-geopolymer composite is cured with microwaves, which in themselves have a much better effect on the LCA assessment than the conventional method of curing in ovens, which is shown in Supplement 2 in Table S3 as a reduction in global warming potential (calculated for geopolymer used in this study, for production of 1 prism, i.e., materials and energy used).
- Emissions: similar to energy reduction (if 5–15 % of waste PUR is used in the composite), the consumption of materials for the preparation of the composite, as well as the emissions resulting from the production of these materials, can be estimated to decrease by 5–15 %, both in air emissions and in the consumption of new raw materials, as well as the water use.
- Use of more sustainable solutions: this refers to all three pillars of sustainable development, i.e., economic, environmental, and social. An economic advantage is obtained with the new composite due to the use of waste materials, which reduces the need to use new raw materials. The environmental benefit is shown in the reduction of waste, which is either deposited in landfills or goes to incineration. They can even be found improperly discarded in nature, where PUR still decomposes as hazardous waste. The social impact is reflected in

society's approach to recycling and the dissemination of this new knowledge, including through open-access publications. For example, just in Germany, about 25 million cans of PU foam are used each year and have to be recycled as hazardous waste separately (Chatzivasileiou, 2020).

## 4. Conclusions

In this study, the potential of grated waste PUR to be incorporated in the geopolymer in a fire-safe manner was shown, i.e. even the addition of 3 g of PUR per 50 g of MK (6 % calculated on mass of MK) did not ignite on a detectable macro-scale level, although PUR still got incinerated in its many chambers, which was confirmed on a micro-scale level. The hindering of flammability of composites was compared to pure PUR and PUR containing organic flame retardants, APP and TATA, which did hinder the flammability of PUR, but not as well as geopolymer. However, PUR without flame retardants closer to the surface can still express its flammable nature, but on a smaller scale compared to PUR that is not protected by an aluminosilicate network and with much more elapsed time after exposure to elevated temperatures.

As expected, the inclusion of (6 % of) PUR lowered the compressive strength of the composite, from ~90 MPa to ~60 MPa when PUR did not contain any organic polymeric fire retardant. However, when fire retardants were present in the PUR structure, the compressive strength of the geopolymer composite decreased to ~40 MPa. The lower mechanical strength of the composites can be for the no-load-bearing products (façade panels) still acceptable; however, for any other building industry product the safe storage of waste PUR should be reconsidered.

Incineration of encapsulated PUR at lower temperatures (up to 500 °C) happens without significant damage to the structure of the embodying material and it creates voids. These voids offer space to all the potential gases released at higher temperatures (somewhere between 750 °C and 1000 °C) that the embodying material (geopolymer) can no longer withstand. However, geopolymer without PUR does not contain these voids; hence it is prone to large crack formation. Therefore, the small addition of grated PUR hinders the temperature-dependent collapse of the material structure and its mechanical strengths.

Nonetheless, permanently encapsulated grated PUR did lower the density of the composite and decrease thermal conductivity, which shows prospects to transform decorative façade panels into decorative insulating façade panels, decreasing the need for additional building envelope layers and decreasing the amount of waste, particularly if the majority of the materials are secondary materials. With the addition of 6 % of PUR per MK, the biggest decrease in thermal conductivity of composites (from 940 to 860 mW/(m·K)) was for PUR containing flame retardant TATA, as it was for geometrical density (from 1.8 to 1.6 kg/l). Both reductions are rather small, compared to pure PUR, but PUR was embedded in the geopolymer only with its intrinsic properties and not also extrinsic because its porous nature was destroyed by grating. This did contain the flammability well but did not offer the geometrical density and thermal conductivity to lower more.

The calculated model of the geometrical density of the composite shows high dependency on the influence of the grating and mass of added PUR: to gain lower thermal conductivity with less added PUR, the geometrical density of the composite has to be lowered with extrinsic

properties of PUR, meaning that porous structure of PUR should not be completely destroyed. In this way, the thickness of walls between PUR inclusions can be wider and offer better individual resistance to external mechanical forces. However, the mapping of mechanical strength dependence on the size and amount of PUR inclusions, which defines the thickness of the load-bearing walls and the distance between the neighbouring walls in the composite, has to be determined in further study.

This study has opened new options for the environmentally friendlier approach to waste management of PUR and a new approach to the design of composites meant for fire-safe building insulation made from porous inclusions by keeping or destroying its structure, that is, by lowering the density of the composite with the geometrical or skeletal density of the inclusion.

With the tight encapsulation of PUR in a non-combustible environment without light, fungi, and microbes, other drawbacks of PUR can also be mitigated, particularly if geopolymer is designed to be antimicrobial. In this way, the 2nd life cycle of PUR can be prolonged in a technically easy and cost-effective way.

## CRediT authorship contribution statement

**Barbara Horvat:** Writing – review & editing, Writing – original draft, Visualization, Validation, Supervision, Software, Resources, Project administration, Methodology, Investigation, Funding acquisition, Formal analysis, Data curation, Conceptualization. **Nataša Knez:** Visualization, Validation, Methodology, Investigation, Formal analysis, Data curation. **Uroš Hribar:** Writing – review & editing, Visualization, Validation, Methodology, Investigation, Formal analysis, Data curation. **Jakob König:** Writing – review & editing. **Branka Mušič:** Writing – review & editing, Writing – original draft, Visualization, Validation, Supervision, Methodology, Investigation, Formal analysis, Data curation, Conceptualization.

## Declaration of competing interest

The authors declare that they have no known competing financial interests or personal relationships that could have appeared to influence the work reported in this paper.

Thermal insulation and flammability of composite waste polyurethane foam encapsulated in geopolymer for sustainable building envelope.

## Data availability

Data is available in the open repository DiRROS with PID http://hdl. handle.net/20.500.12556/DiRROS-18221.

## Acknowledgement

**Appendix GSupplementary data**

Supplementary data to this article can be found online at https://doi.org/10.1016/j.jclepro.2024.141387.

**Appendix A**

For comparison of results obtained using cone calorimeter and atmosFTIR, time-dependent datasets ($x_i(t)$) for sample i and parameter $x$ were factorised by the biggest mass among samples, namely, $MK_b$, and divided by its own mass, $m_i$. In addition to factorisation, negative results at time $t_j$ ($j$ goes from 0 to the last acquisition) were filtered (mass is not negative):

$$x_i^{MK_b}(t) = x_i(t) \bullet \frac{m_{MK_b}}{m_i} \bullet \begin{cases} 0, x_i(t_j) < 0 \\ 1, x_i(t_j) \geq 0 \end{cases}, \qquad \text{Eq. (A.1)}$$

where $x_i^{MK_b}(t)$ is the dataset where all tested samples would have mass $m_{MK_b}$.

To compare fire results when the amount of fuel is the same, $x_i^{PUR}(t)$, datasets were multiplied by the chosen mass of PUR ($m_{PUR}$), which was set to 10 g, and divided by the individual mass of the sample's fuel $m_{i\text{-}PUR}$:

$$x_i^{PUR}(t) = x_i(t) \bullet \frac{m_{PUR}}{m_{i-PUR}} \bullet \begin{cases} 0, x_i(t_j) < 0 \\ 1, x_i(t_j) \geq 0 \end{cases}, \qquad \text{Eq. (A.2)}$$

where negative values were filtered, and where $m_{i\text{-}PUR}$ is:

$$m_{i-PUR} = \begin{cases} m_i, if\ sample\ is\ PUR \\ m_i \bullet \dfrac{m_{PURinAAM}}{m_{MK} + m_{Alkali} + m_{H2O}}, if\ sample\ is\ composite\ of\ geopolymer\ and\ PUR \end{cases}, \qquad \text{Eq. (A.3)}$$

where data for $\frac{m_{PURinAAM}}{m_{MK}+m_{Alkali}+m_{H2O}}$ is taken from Table 1 ($m_{PURinAAM} = 3\ g$, $m_{MK} = 50\ g$, $m_{Alkali} = 33\ g$ and $m_{H2O} = 0$, i.e., no additional water was added).

**Appendix B**

The samples did not show any visual difference between being irradiated with microwaves (100 W, 1 min) just after moulding and being solely cured at room conditions (Fig. B1), not much difference was observed between samples with only 1 g and up to 5 g of added PUR$_{mix}$ (Fig. B1).
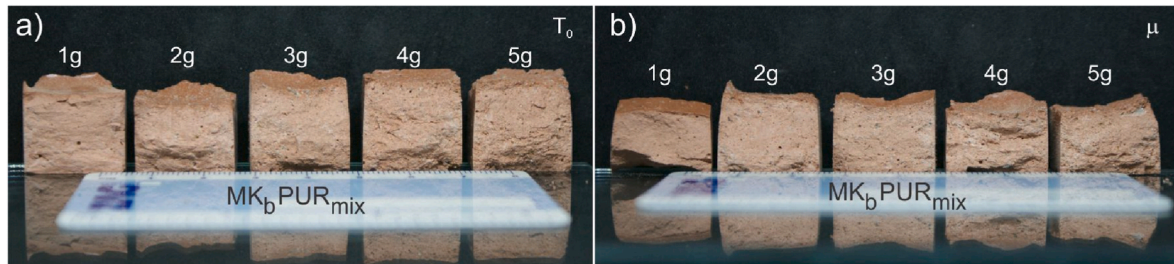


**Fig. B.1.** Photographs of cross-sections of composites containing 1–5 g of grated PUR$_{mix}$, a) treated at room conditions, and b) irradiated with microwaves.

Furthermore, composites with 3 g of PUR-0, PUR-1, or PUR-2 did not differ from geopolymer without PUR (MK$_b$) at room conditions (Fig. B2). However, there was a big difference between samples with and without PUR already at 250 °C, when PUR started to deteriorate, as shown in SEM micrographs (Fig. 5). Addition of the flame retardants in PUR did not visually influence the composite with PUR at any temperature (Fig. B2 b, c and d). Moreover, composites that initially had PUR in the structure had higher mechanical strengths (compressive, but especially bending strength) at 1000 °C, although with lower $\rho_G$ and $\rho_B$ (Fig. 6 b), because fewer and less prominent new macro cracks were formed (Fig. B2). After the incineration of PUR (which occurred below 500 °C) voids (initially containing PUR) were available for released gasses (Horvat and Ducman, 2020). While geopolymer without PUR (MK$_b$) had a "fuller" initial structure (total porosity was lower, Fig. 6 a), the release of gasses at 1000 °C (Fig. B2 a) increased the pressure from the inside of the structure and formed large cracks (MIP measures pore entries from 3 nm to 1 mm at its best, and thus, those cracks were not detected). However, the remaining structure was not filled with voids, and thus, the $\rho_G$ at 1000 °C was higher than for samples containing PUR.
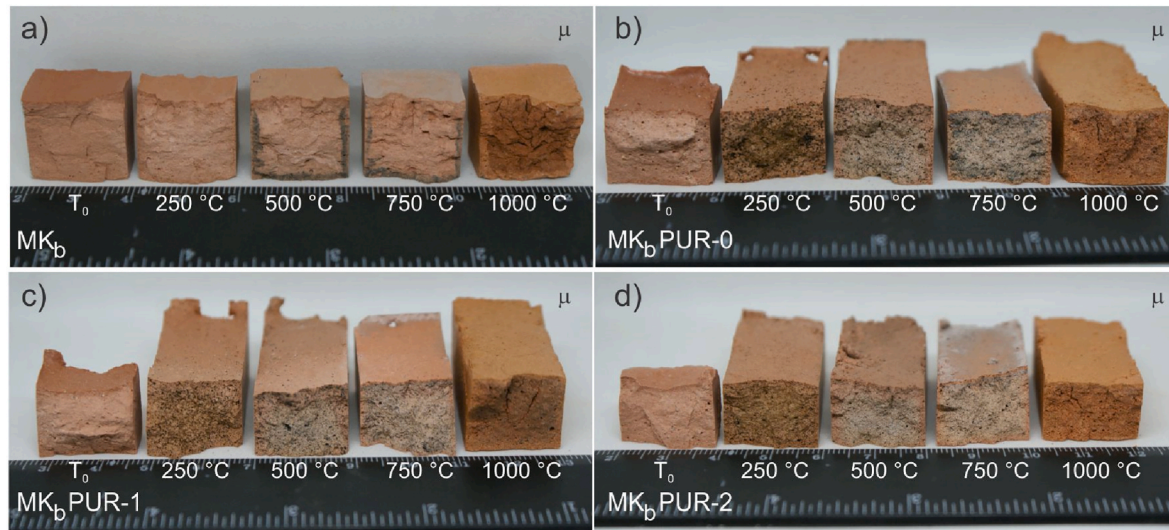
**Fig. B.2.** Photographs of a) geopolymer $MK_b$ and composites with 3 g of b) PUR-0, c) PUR-1, and d) PUR-2 treated at selected temperatures.

## Appendix C

While SEM micrographs at larger magnification show only organic inclusions and ASN deterioration upon the heat treatment (Fig. 5), they do not represent overall statistical data and can be misleading. Therefore, SEM micrographs acquired at low magnification are provided in Fig. C1 (excluding positions with the biggest cracks that are seen on the photographs in Fig. B2). When comparing the structures of composites at room conditions, the interior of $MK_b$ is the "fullest" (its total porosity is the lowest, Fig. 8), while grated PUR is randomly integrated all around geopolymer structure and remains present at least up to 250 °C. At 500 °C, there are no visible remains of PUR, instead, only large voids are present where grated PUR was located, with smooth surface where geopolymer was in contact with PUR. Pores (voids) in composites containing PUR are placed randomly around the structure (just like PUR was), while geopolymer without PUR contains only elongated cracks, which are already present at room conditions but become more prominent with an increase in temperature (mechanical strength decreases, Fig. 4, and total porosity increases, Fig. 8, with elevated temperature, at least at 500 °C and above). Deterioration of the inorganic part of the composite at 1000 °C on a large scale is visible as the small circular/spherical holes in the structure all around the sample cross-section, while geopolymer without PUR shows only the beginning of the deterioration (squares in Fig. C1 e). $MK_b$ structure is much less open than composites that initially contained PURs, i.e., oxygen needed for oxidation (or any other reaction needing atmospheric gasses) does not have such easy and uniform access to the interior of the material.
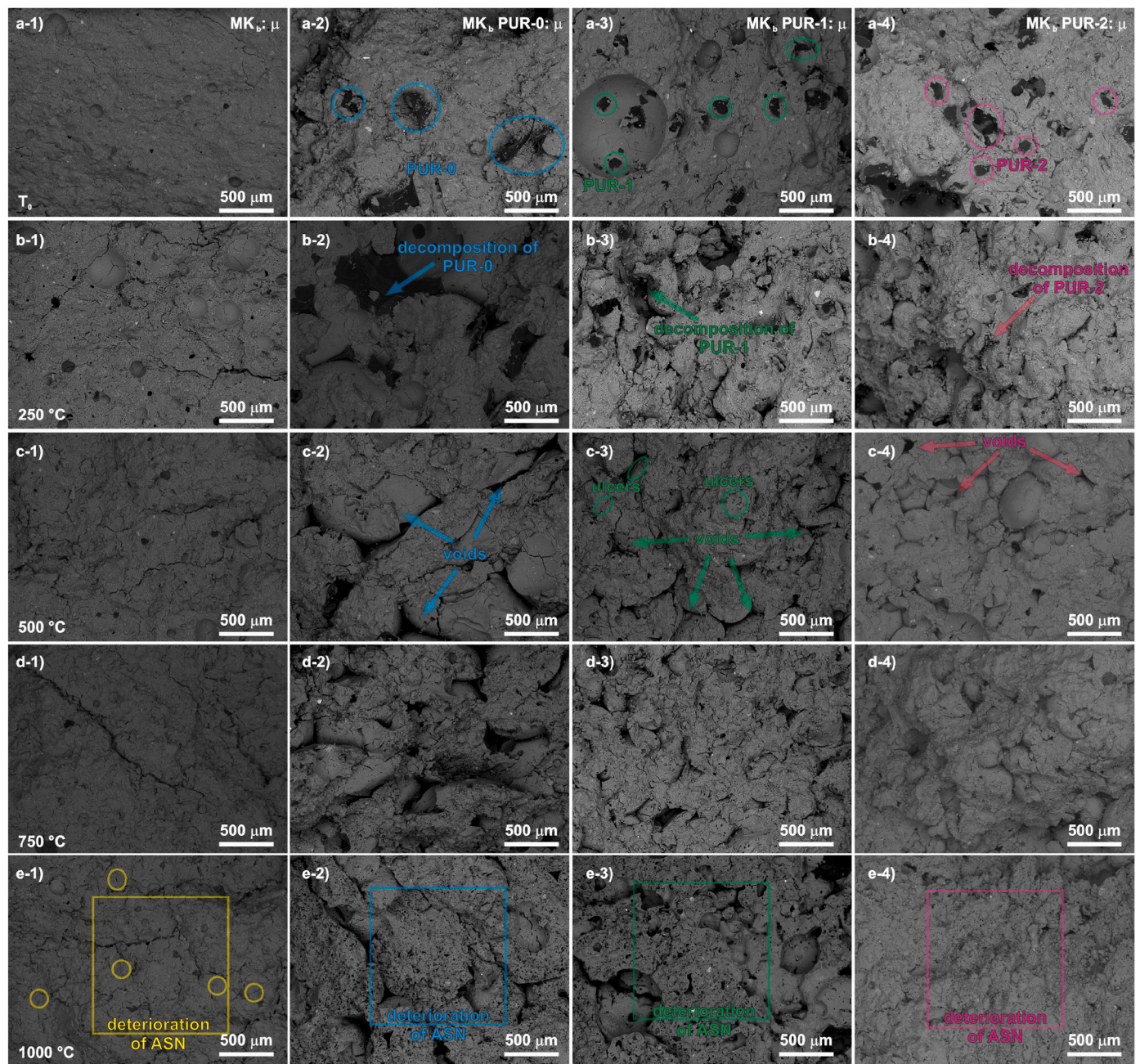
**Fig. C.1.** SEM micrographs (50-times magnified) of 1) geopolymer $MK_b$ and composites with incorporated 2) PUR-0, 3) PUR-1, and 4) PUR-2 treated at selected temperatures (a) room conditions, b) 250 °C, c) 500 °C, d) 750 °C and e) 1000 °C).

## Appendix D

Chemical (FTIR) and mineralogical (XRD) changes in the composites upon the heat treatment are shown in Fig. D.1 and Fig. D.2, respectively. While the inclusion of APP and TATA in PUR is evident in FTIR and XRD (marked with ellipse and rectangle; Fig. D.1 and D.2, a)), their amounts in geopolymer are just too small for the FTIR and XRD to detect them (Fig. D.1 and D.2, d, e, f, patterns not treated at elevated temperatures). In the case of XRD, they cannot be distinguished from pattern without PUR (Fig. D.2 c), at any temperature, implying that the selected small amount of PUR included in the composite did not affect the mineralogy of the composite, nor the mineralogical stability of the inorganic material upon the heat treatment. The change in the mineralogy was detected for all samples at 1000 °C (formation of mineral nepheline); however, this could have occurred somewhere above 750 °C and below 1000 °C, but not necessarily at the same temperature for all composites.

By contrast, the presence of the organic material can be noticed in FTIR of all composites with PUR (located in the black dashed square that overlaps with the water peak and also with the ASN peak). Nonetheless, the amount of added organic materials was too low to be able to determine which organic compound was present in the system. The "organic" peaks cannot be detected at 500 °C and above (deterioration of PURs was confirmed also by SEM analysis, Fig. 5 and Fig. C1), while the peak for $H_2O$ is not detected anymore at 250 °C (in $MK_b$ sample, while composites containing PURs show the "water" peak, but it overlaps with the "organic" peaks). From our previous study, the PURs started degrading at ~250 °C, while its decomposition ended above 600 °C for PUR-0 and PUR-2; however, for PUR-1 the decomposition ended above 800 °C (Mušič et al., 2023a).

Nonetheless, grated PURs were incorporated in alkali media (geopolymer), which influenced PUR with/without fire retardants and decreased decomposition temperature (substrates/soil influences the decomposition rate of organic material in nature (Conant et al., 2011)).

The most concerning outcome from this study is that the position of the "ASN" peak (Si–O–Si and Si–O–Al bonds for MK; and Si–O–Si bonds for the alkali used) for geopolymers produced from materials containing organic materials might be questionable because organic materials do show peaks at the location of the "ASN" peak obtained in the current study. The presence of organic compounds can be seen in the "ASN" peek as additional inflection points between obvious minima and maxima (an example is in the red circled area in Fig. D1). Those peaks can shift "ASN" peak minima. When knowing which organic compound is in the mixture (if it did not react with alkali) and its exact amount, deconvolution of the "ASN" peak is theoretically possible. However, the overlapping peaks are particularly concerning when waste materials are used as precursors (instead of MK) where the organic compounds and their amounts are not known. In this case, deconvolution is not possible and evaluation of the position of the "ASN" peak minima should not be considered.
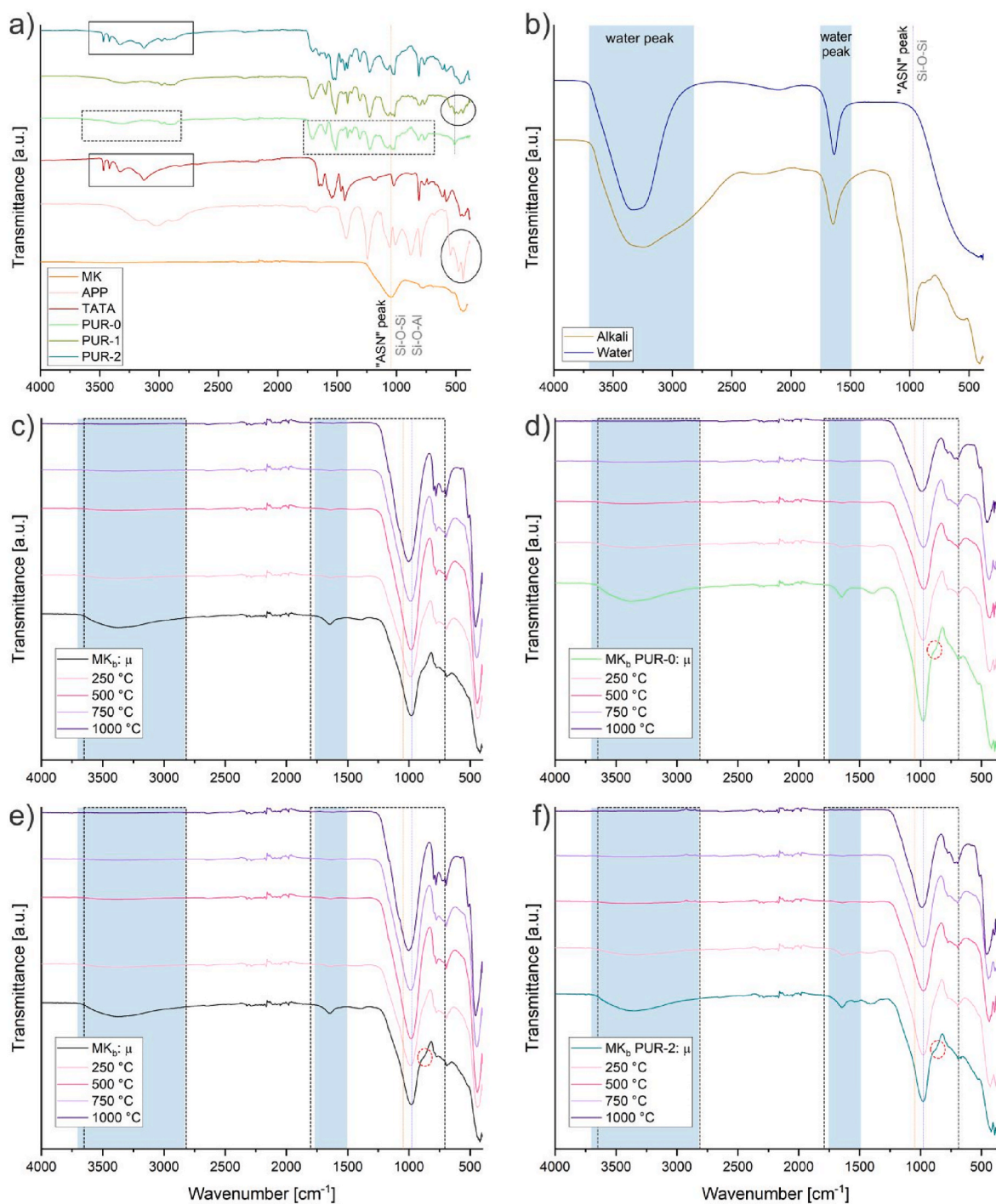


**Fig. D.1.** FTIR spectra of a) solid and b) liquid ingredients used in the synthesis of geopolymer c) MK$_b$, and composites with encapsulated d) PUR-0, e) PUR-1, and f) PUR-2 treated at selected temperatures. Additional labels: positions of the water peak (blue square), "ASN" peak (of MK, orange vertical line, and of alkali, blue vertical line), peak patterns of organic compounds (APP, black ellipse, TATA, black rectangle, PUR-0, black dashed rectangle), inflection point (red dashed ellipse).
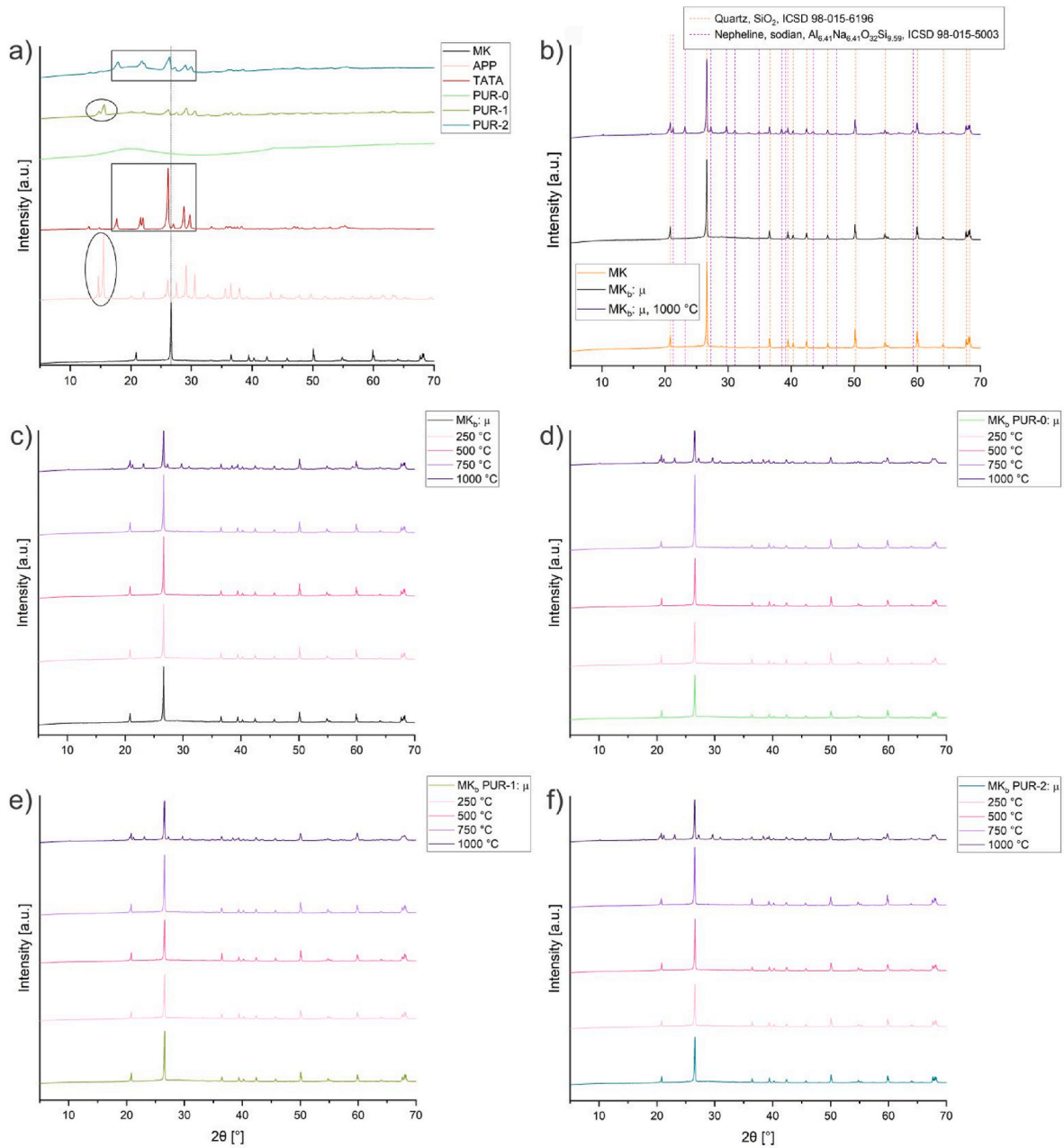
**Fig. D.2.** XRD of a) solid ingredients used in the synthesis of geopolymer, b) solved patterns for MK, $MK_b$ and $MK_b$ treated at 1000 °C, c) $MK_b$, and composites with encapsulated d) PUR-0, e) PUR-1, and f) PUR-2 treated at selected temperatures.

## Appendix E

The theoretical $\rho_G$ of the composite ($MK_b$ PUR-0, $MK_b$ PUR-1, and $MK_b$ PUR-2, $\rho_{composite}$) was calculated using the measured $\rho_G$ of the composite without inclusion ($MK_b$, $\rho_{body}$) and $\rho_G$ or $\rho_S$ of inclusion (PUR-0, PUR-1 and PUR-2, $\rho_{inclusion}$):

$$\rho_{composite} = \frac{m_{body} + m_{inclusion}}{V_{body} + V_{inclusion}} = \rho_{body} \bullet \rho_{inclusion} \bullet \frac{1 + m_{inclusionND}}{\rho_{inclusion} + \rho_{body} \bullet m_{inclusionND}},$$

Eq. (E.1)

where in Eq. (E.1) were introduced: densities $\rho_{body} = \frac{m_{body}}{V_{body}}$ and $\rho_{inclusion} = \frac{m_{inclusion}}{V_{inclusion}}$, and dimensionless ratio of inclusion and of ingredients for the body of the composite (with or without water) $m_{inclusionND} = \frac{m_{inclusion}}{m_{body\_ingredients}}$.

The calculated $\rho_G$ of the composites in dependence on the mass of the inclusion ($m_{PUR}$, going from 0 to 50 g, where 50 g equals the mass of the precursor in the experiment, $m_{MK}$), are shown in Fig. E1. A significant difference exists in the density of the composite regarding the quality of the PUR grating, i.e., well-grated PUR decreases composite density less than PUR that retains the porous structure. The former contributes to the composite density through its $\rho_S$ (S in Fig. E1) and the latter through much lower $\rho_G$ (G in Fig. E1). To get close to the lowest limit value of $\rho_G$ of the composite, i. e., to the density of the inclusion, the need for the addition of inclusions with intact porous structure is much lesser than if the porous structure is destroyed. Although in theory, with the sufficient addition of well-grated PUR, the lowest $\rho_G$ limit value of the composite can be reached, this is not possible with the geopolymer mixture used in the current study (the surface area of the well-grated PUR in contact with liquid/slurry is bigger than in case of poorly grated highly porous material when the slurry does not enter its inner structure).

The difference in the densities of the composites if the water evaporates (calculated on all solid material without inclusions) or remains in the system (calculated on slurry without inclusions) is not significant, compared to the difference between the well- and the poorly-grated PUR. As $\rho_G$ of the composite where well-grated PUR was used is between the values obtained with all the water still present and all evaporated, $\rho_G$ of the composite of random quality of grating of the PUR can be between well-grated (S) and poorly-grated (G) curve.
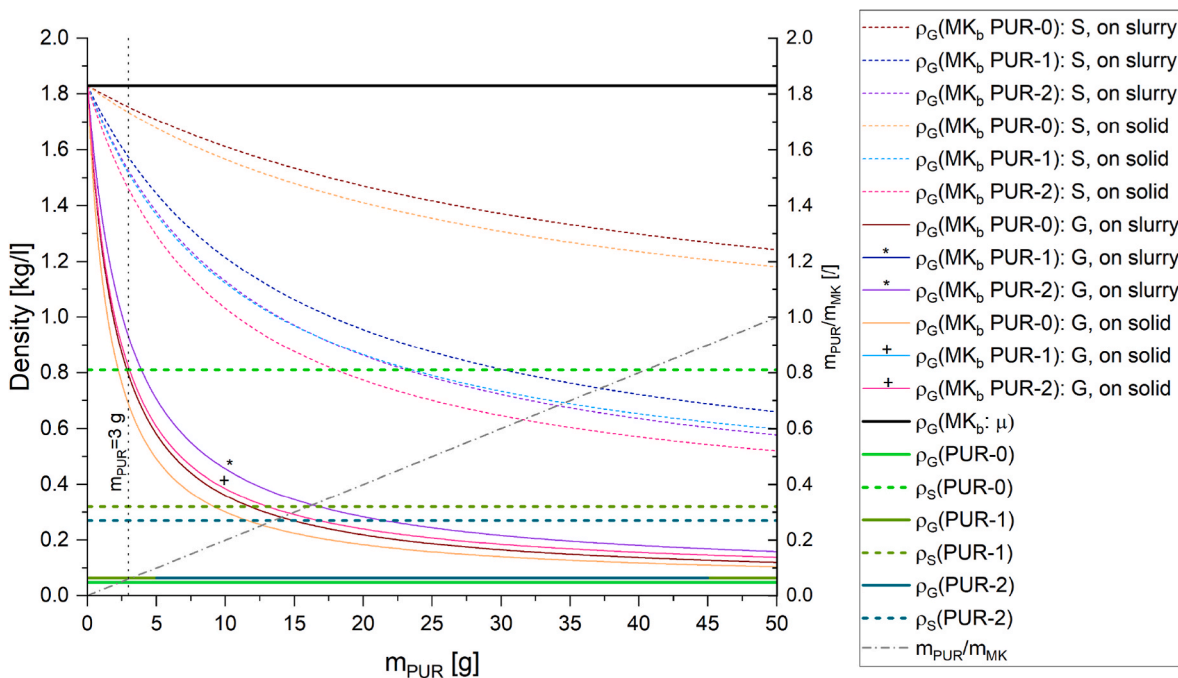


**Fig. E.1.** Dependence of $\rho_G$ of the composite on the mass of the inclusion, with boundaries $MK_b$, PUR-0, PUR-1, PUR-2 ($\rho_G$ of PUR-1 and PUR-2 overlap), and with the ratio of the mass of inclusion to the mass of MK (50 g). * and + are showing the overlapping curves.

## Appendix F

Measuring the complex dielectric constant of liquids with VNA requires only dipping the probe into the liquid. When the liquid sample is replaced by a solid, and if the solid is a "fine" and non-hollow powder, the procedure of measuring the complex dielectric constant is as if the powder was a liquid. However, highly porous bulk material (that can not be milled to avoid chemical changes owing to the potential increase of the heat while milling) represents a challenge shown in Fig. F1. The sinusoidal response was observed only when (additional) force was applied by the probe onto the dry sample (to get more contact of the probe and material), i.e., onto the PUR cube or PUR's outer wall. This sinusoid cannot be compared with porosity, because the pores of PUR-0 are different from the pores of PUR-1 and PUR-2 (Fig. 1), while sinusoidal behaviour is comparable. Moreover, it cannot be compared with the sample size, because the sample size of the cube was ~5 cm in height, while the thickness of the wall was ~1 mm. Therefore, as valid results, only the measurements without the probe being firmly pressed onto the sample surface were considered. However, PUR would have to be gently grated into even finer powder to be able to determine how good the measurement is if the probe is in contact with porous bulk material or in powder-like material and how "fine" the powder has to be.
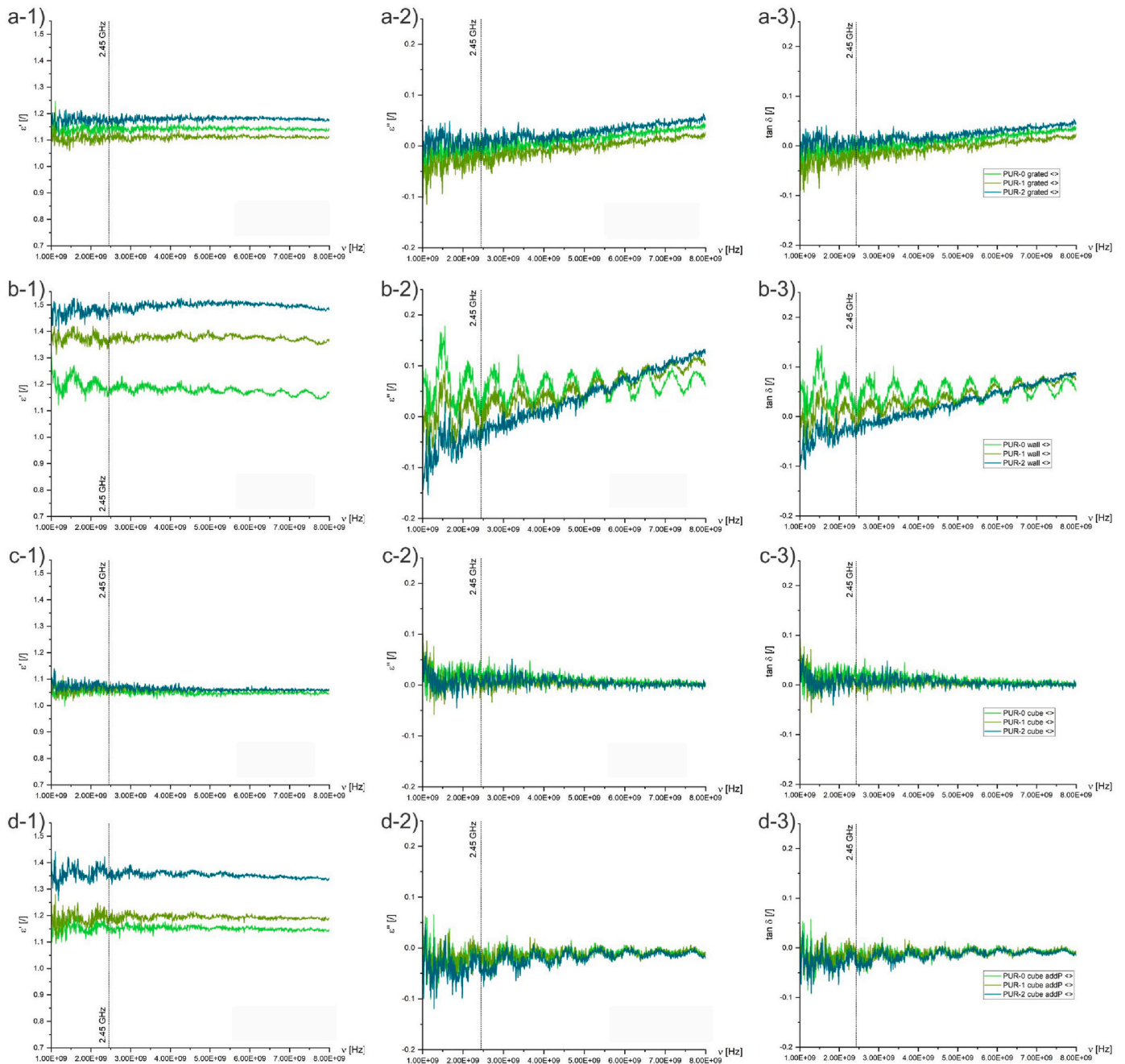
**Fig. F.1.** Frequency-dependent complex dielectric constant ($\varepsilon' + i \bullet \varepsilon''$) and losses ($\tan \delta$) for PUR-0, PUR-1, and PUR-2: a) grated (measured like powder sample), b) measured by placing the probe with applied force onto the outer PUR wall, c) measured by gently placing the probe onto the inner layer of the PUR and d) with applied force. 1) Real ($\varepsilon'$) and 2) imaginary part ($\varepsilon''$) of the complex dielectric constant, and 3) dissipation factor.

## References

Ahmed, H.U., Mohammed, A.S., Faraj, R.H., Abdalla, A.A., Qaidi, S.M.A., Sor, N.H., Mohammed, A.A., 2023. Innovative modeling techniques including MEP, ANN and FQ to forecast the compressive strength of geopolymer concrete modified with nanoparticles. Neural Comput. Appl. 35, 12453–12479. https://doi.org/10.1007/s00521-023-08378-3.

Albidah, A., Alsaif, A., Abadel, A., Abbas, H., Al-Salloum, Y., 2022. Role of recycled vehicle tires quantity and size on the properties of metakaolin-based geopolymer rubberized concrete. J. Mater. Res. Technol. 18, 2593–2607. https://doi.org/10.1016/j.jmrt.2022.03.103.

Atienza, E.M.-, Ongpeng, J.M.C., 2022. Environmental impact and cost comparison of different Partition walls. Chem. Eng. Trans. 94, 691–696. https://doi.org/10.3303/CET2294115.

Beglarigale, A., Seki, Y., Demir, N.Y., Yazıcı, H., 2018. Sodium silicate/polyurethane microcapsules used for self-healing in cementitious materials: Monomer optimization, characterization, and fracture behavior. Constr Build Mater 162, 57–64. https://doi.org/10.1016/j.conbuildmat.2017.11.164.

Bergamonti, L., Taurino, R., Cattani, L., Ferretti, D., Bondioli, F., 2018. Lightweight hybrid organic-inorganic geopolymers obtained using polyurethane waste. Constr Build Mater 185, 285–292. https://doi.org/10.1016/j.conbuildmat.2018.07.006.

Chatzivasileiou, V., 2020. Recycling polyurethane foam in pressurised containers [WWW Document]. European circular economy Stakeholder Platform. URL. https://circulareconomy.europa.eu/platform/en/good-practices/recycling-polyurethane-foam-pressurised-containers, 1.22.24.

Chen, Y.X., Klima, K.M., Brouwers, H.J.H., Yu, Q., 2022. Effect of silica aerogel on thermal insulation and acoustic absorption of geopolymer foam composites: the role of aerogel particle size. Compos. B Eng. 242, 110048 https://doi.org/10.1016/j.compositesb.2022.110048.

Chen, Z., Lee, S.-J., 2018. Study on properties of geopolymer-polyurethane sponge composite. J. Ceram. Process. Res. 19, 419–423.

Conant, R.T., Ryan, M.G., Ågren, G.I., Birge, H.E., Davidson, E.A., Eliasson, P.E., Evans, S.E., Frey, S.D., Giardina, C.P., Hopkins, F.M., Hyvönen, R., Kirschbaum, M.U. F., Lavallee, J.M., Leifeld, J., Parton, W.J., Megan Steinweg, J., Wallenstein, M.D., Martin Wetterstedt, J.Å., Bradford, M.A., 2011. Temperature and soil organic matter decomposition rates - synthesis of current knowledge and a way forward. Glob. Change Biol. 17, 3392–3404. https://doi.org/10.1111/j.1365-2486.2011.02496.x.

Daminev, R.R., 2020. The main factors, influencing the processes in the microwave field. IOP Conf. Ser. Mater. Sci. Eng. 919, 022043 https://doi.org/10.1088/1757-899X/919/2/022043.

Davidovits, J., 1989. Geopolymers and geopolymeric materials. J. Therm. Anal. 35, 429–441. https://doi.org/10.1007/BF01904446.

Deja, J., 2002. Immobilization of Cr6+, Cd2+, Zn2+ and Pb2+ in alkali-activated slag binders. Cem. Concr. Res. 32, 1971–1979. https://doi.org/10.1016/S0008-8846(02) 00904-3.

Dos Reis Ferreira, R.A., Gratão, L.S., De Castro Motta, L.A., 2024. Evaluation and optimization of the replacement of fine aggregate by waste tire rubber in geopolymer Mortar with metakaolin. Mech. Compos. Mater. https://doi.org/10.1007/s11029-023-10168-w.

Ducman, V., Korat, L., 2016. Characterization of geopolymer fly-ash based foams obtained with the addition of Al powder or H2O2 as foaming agents. Mater. Charact. 113, 207–213. https://doi.org/10.1016/j.matchar.2016.01.019.

Duxson, P., Provis, J.L., Lukey, G.C., Mallicoat, S.W., Kriven, W.M., van Deventer, J.S.J., 2005. Understanding the relationship between geopolymer composition, microstructure and mechanical properties. Colloids Surf., A 269, 47–58. https://doi.org/10.1016/j.colsurfa.2005.06.060.

Fan, M., Fu, F., 2017. Advanced High Strength Natural Fibre Composites in Construction. Elsevier, Amsterdam, Netherlands. https://doi.org/10.1016/C2014-0-03942-1.

Fernandez-Jimenez, A., Macphee, D.E., Lachowski, E.E., Palomo, A., 2005. Immobilization of cesium in alkaline activated fly ash matrix. J. Nucl. Mater. 346, 185–193. https://doi.org/10.1016/j.jnucmat.2005.06.006.

Garces, J.I.T., Tan, R.R., Beltran, A.B., Ongpeng, J.M.C., Promentilla, M.A.B., 2021. Environmental life cycle assessment of alkali-activated material with different Mix designs and self-healing agents. Chem. Eng. Trans. 88, 835–840. https://doi.org/10.3303/CET2188139.

Gogoi, R., Alam, M., Khandal, R., 2014. Effect of increasing NCO/OH molar ratio on the physicomechanical and thermal properties of isocyanate terminated polyurethane prepolymer. J. Basic Appl. Sci. 3, 118–123. https://doi.org/10.14419/ijbas.v3i2.2416.

Grolms, M., 2019. A New Method to Chemically Recycle Polyurethane Waste [WWW Document]. Advanced Science News. URL https://www.advancedsciencenews.com/solution-for-polyurethane-waste/. (Accessed 3 December 2023).

Grünbauer, H., Bicerano, Clavel, Daussin, R., De Vos, H., Elwell, M., Kawabata, Kramer, Latham, D., Martin, C., Moore, S., Obi, B., Parenti Schrock, A., Van Den, Bosch, 2004. Rigid polyurethane foams. In: Lee, S., Ramesh, N. (Eds.), Polymeric Foams - Mechanisms and Materials. CRC Press, London, UK, p. 360. https://doi.org/10.1201/9780203506141.ch7.

Guangren, Q., 2002. Improvement of metakaolin on radioactive Sr and Cs immobilization of alkali-activated slag matrix. J. Hazard Mater. 92, 289–300. https://doi.org/10.1016/S0304-3894(02)00022-5.

Günther, M., Lorenzetti, A., Schartel, B., 2018. Fire Phenomena of rigid polyurethane foams. Polymers 10, 1166. https://doi.org/10.3390/polym10101166.

Hassan, A., Rashid, Y., Mourad, A.-H.I., Ismail, N., Laghari, M.S., 2019. Thermal and structural characterization of geopolymer-coated polyurethane foam—phase change material Capsules/geopolymer concrete composites. Materials 12, 796. https://doi.org/10.3390/ma12050796.

He, L., Deng, L., Li, Y., Luo, H., He, J., Huang, S., Chen, H., 2018. Wide-angle microwave absorption performance of polyurethane foams combined with cross-shaped metamaterial absorber. Results Phys. 11, 769–776. https://doi.org/10.1016/j.rinp.2018.10.021.

Horvat, B., Ducman, V., 2020. Influence of particle size on compressive strength of alkali activated Refractory materials. Materials 13, 2227. https://doi.org/10.3390/ma13102227.

Horvat, B., Ducman, V., 2019. Potential of green Ceramics waste for alkali activated foams. Materials 30. https://doi.org/10.3390/ma12213563.

Horvat, B., Mušič, B., 2023. Waste rubber incorporated in the alkali-activated Metakaolin's aluminosilicate network enhanced by microwave irradiation. In: 6th International Conference on Technologies & Business Models for Circular Economy: Conference Proceedings. Presented at the International Conference on Technologies & Business Models for Circular Economy, Slovenia. Portorož https://doi.org/10.18690/um.fkkt.3.2023.

Horvat, B., Mušič, B., Pavlin, M., Ducman, V., 2023. Microwave irradiation of alkali-activated metakaolin slurry. In: Presented at the International Conference on Technologies & Business Models for Circular Economy. University of Maribor Press, Slovenia, Portorož, pp. 9–24. https://doi.org/10.18690/um.fkkt.1.2023.2.

Horvat, B., Mušič, B., Pavlin, M., Ducman, V., 2022a. Microwave irradiation of alkali-activated metakaolin slurry. In: Presented at the 5th International Conference on Technologies & Business Models for Circular Economy, Slovenia, Portorož. https://doi.org/10.18690/um.fkkt.6.2022.

Horvat, B., Pavlin, M., Ducman, V., 2022b. Influence of microwaves in the early stage of alkali activation on the mechanical strength of alkali-activated materials. Ceram. Int. https://doi.org/10.1016/j.ceramint.2022.12.133.

Jow, J., Lai, S.-Y., Zhao, Y., Cai, X., 2015. Fly ash-based geopolymer foam technology for thermal insulation and fire protection applications. Proceedings of the 2015. World of Coal Ash (WOCA, USA, Nashville, TN, pp. 5–7.

Khalil, M.Y., Merz, E., 1994. Immobilization of intermediate-level wastes in geopolymers. J. Nucl. Mater. 211, 141–148. https://doi.org/10.1016/0022-3115 (94)90364-6.

Kheimi, M., Aziz, I.H., Abdullah, M.M.A.B., Almadani, M., Abd Razak, R., 2022. Waste material via Geopolymerization for heavy-Duty application: a review. Materials 15, 3205. https://doi.org/10.3390/ma15093205.

Kohout, J., Koutník, P., 2020. Effect of filler type on the thermo-mechanical properties of Metakaolinite-based geopolymer composites. Materials 13, 2395. https://doi.org/10.3390/ma13102395.

Łach, M., Korniejenko, K., Mikuła, J., 2016. Thermal insulation and thermally resistant materials made of geopolymer foams. Procedia Eng. 151, 410–416. https://doi.org/10.1016/j.proeng.2016.07.350.

Le Roy, R., Parant, E., Boulay, C., 2005. Taking into account the inclusions' size in lightweight concrete compressive strength prediction. Cem. Concr. Res. 35, 770–775. https://doi.org/10.1016/j.cemconres.2004.06.002.

Longhi, M.A., Rodríguez, E.D., Walkley, B., Zhang, Z., Kirchheim, A.P., 2020. Metakaolin-based geopolymers: relation between formulation, physicochemical properties and efflorescence formation. Compos. B Eng. 182, 107671 https://doi.org/10.1016/j.compositesb.2019.107671.

Marvila, M.T., Azevedo, A.R.G. de, Vieira, C.M.F., 2021. Reaction mechanisms of alkali-activated materials. Rev. IBRACON Estrut. Mater. 14, e14309 https://doi.org/10.1590/s1983-41952021000300009.

Merillas, B., Martín-de León, J., Villafañe, F., Rodríguez-Pérez, M.Á., 2022. Optical properties of polyisocyanurate–polyurethane aerogels: study of the scattering mechanisms. Nanomaterials 12, 1522. https://doi.org/10.3390/nano12091522.

Mohajerani, A., Suter, D., Jeffrey-Bailey, T., Song, T., Arulrajah, A., Horpibulsuk, S., Law, D., 2019. Recycling waste materials in geopolymer concrete. Clean Technol. Environ. Policy 21, 493–515. https://doi.org/10.1007/s10098-018-01660-2.

Moradikhou, A.B., Esparham, A., Jamshidi Avanaki, M., 2020. Physical & mechanical properties of fiber reinforced metakaolin-based geopolymer concrete. Constr Build Mater 251, 118965. https://doi.org/10.1016/j.conbuildmat.2020.118965.

Mušič, B., Horvat, B., Knez, N., 2023a. Influence of polymeric flame retardants on the flammability and mechanical-physical properties of polyurethane and alkali-activated foams. In: 6th International Conference on Technologies & Business Models for Circular Economy: Conference Proceedings. Presented at the International Conference on Technologies & Business Models for Circular Economy. https://doi.org/10.18690/um.fkkt.3.2023.

Mušič, B., Horvat, B., König, J., Hribar, U., 2023b. Zaviralci ognja v negorljivih fasadnih elementih (Fire retardants in non-combustible facade elements). Finance, Gradbeništvo 16, 56–58.

Mušič, B., Knez, N., Bernard, J., 2022. Flame retardant behaviour and physical-mechanical properties of polymer Synergistic systems in rigid polyurethane foams. Polymers 14, 4616. https://doi.org/10.3390/polym14214616.

Nadi, M., Allaoui, D., Majdoubi, H., Hamdane, H., Haddaji, Y., Mansouri, S., Tamraoui, Y., Manoun, B., Hannache, H., Oumam, M., 2023. Effect of natural graphite additions on the microstructural and mechanical behavior of metakaolin based geopolymer materials. J. Build. Eng. 78, 107562 https://doi.org/10.1016/j.jobe.2023.107562.

Nikolić, V., Komljenović, M., Džunuzović, N., Ivanović, T., Miladinović, Z., 2017. Immobilization of hexavalent chromium by fly ash-based geopolymers. Compos. B Eng. 112, 213–223. https://doi.org/10.1016/j.compositesb.2016.12.024.

Nikolić, V., Komljenović, M., Marjanović, N., Bašćarević, Z., Petrović, R., 2014. Lead immobilization by geopolymers based on mechanically activated fly ash. Ceram. Int. 40, 8479–8488. https://doi.org/10.1016/j.ceramint.2014.01.059.

Pandya, J., Shah, S., Dave, S., 2017. Feasibility of Utilization of industrial polyurethane (PU) rubber waste in geopolymer concrete. Presented at the ICRISET2017. In: International Conference on Research and Innovations in Science, Engineering and Technology. Selected Papers in Civil Engineering. https://doi.org/10.29007/2xq2, 285–278.

Pavlin, M., Horvat, B., Ducman, V., 2022. Preparation of façade panels based on alkali-activated waste mineral wool, their characterization, and durability aspects. Int. J. Appl. Ceram. ijac, 13998 https://doi.org/10.1111/ijac.13998.

Podolsky, Z., Liu, J., Dinh, H., Doh, J.H., Guerrieri, M., Fragomeni, S., 2021. State of the art on the application of waste materials in geopolymer concrete. Case Stud. Constr. Mater. 15, e00637 https://doi.org/10.1016/j.cscm.2021.e00637.

Prud'homme, E., Joussein, E., Rossignol, S., 2015. Use of silicon carbide sludge to form porous alkali-activated materials for insulating application. Eur. Phys. J. Spec. Top. 224, 1725–1735. https://doi.org/10.1140/epjst/e2015-02494-7.

Qaidi, S., Yahia, A., Tayeh, B.A., Unis, H., Faraj, R., Mohammed, A., 2022. 3D printed geopolymer composites: a review. Mater. Today Sustain. 20, 100240 https://doi.org/10.1016/j.mtsust.2022.100240.

Sá Ribeiro, R.A., 2017. A review of particle- and fiber-reinforced metakaolin-based geopolymer composites. J. Ceram. Sci. Technol. https://doi.org/10.4416/JCST2017-00048.

Sarazin, J., Davy, C.A., Bourbigot, S., Tricot, G., Hosdez, J., Lambertin, D., Fontaine, G., 2021. Flame resistance of geopolymer foam coatings for the fire protection of steel. Compos. B Eng. 222, 109045 https://doi.org/10.1016/j.compositesb.2021.109045.

Skariah Thomas, B., Yang, J., Bahurudeen, A., Chinnu, S.N., Abdalla, J.A., Hawileh, R.A., Hamada, H.M., 2022. Geopolymer concrete incorporating recycled aggregates: a comprehensive review. Clean. Mater. 3, 100056 https://doi.org/10.1016/j.clema.2022.100056.

Škvára, F., 2007. Alkali Activated Material - Geopolymer, vol. 16. Department of Glass and Ceramics Faculty of Chemical Technology.

Szycher, M., 2013. Szycher's Handbook of Polyurethanes, second ed. CRC Press, Taylor & Francis Group, Florida, USA.

Tamura, H., 2006. Microwave dielectric losses caused by lattice defects. J. Eur. Ceram. Soc. 26, 1775–1780. https://doi.org/10.1016/j.jeurceramsoc.2005.09.080.

Traven, K., Wisniewski, W., Češnovar, M., Ducman, V., 2022. Microstructural characterization of alkali-activated composites of lightweight aggregates (LWAs) embedded in alkali-activated foam (AAF) Matrices. Polymers 14, 1729. https://doi.org/10.3390/polym14091729.

Yang, T.-Y., Chou, C.-C., Chien, C.-C., 2012. The effects of foaming agents and Modifiers on a Foamed-geopolymer. The 2012 World Congress on Advances in Civil, Environmental, and Materials Research (ACEM' 12) 10.

Yue, Y., 2022. The hardest amorphous material. Natl. Sci. 9, nwab203 https://doi.org/10.1093/nsr/nwab203.

Yunsheng, Z., Wei, S., Qianli, C., Lin, C., 2007. Synthesis and heavy metal immobilization behaviors of slag based geopolymer. J. Hazard Mater. 143, 206–213. https://doi.org/10.1016/j.jhazmat.2006.09.033.

Zaid, O., Martínez-García, R., Abadel, A.A., Fraile-Fernández, F.J., Alshaikh, I.M.H., Palencia-Coto, C., 2022. To determine the performance of metakaolin-based fiber-reinforced geopolymer concrete with recycled aggregates. Archiv.Civ.Mech.Eng 22, 114. https://doi.org/10.1007/s43452-022-00436-2.

Zhang, Z., Provis, J.L., Reid, A., Wang, H., 2015. Mechanical, thermal insulation, thermal resistance and acoustic absorption properties of geopolymer foam concrete. Cem. Concr. Res. 62, 97–105. https://doi.org/10.1016/j.cemconcomp.2015.03.013.